An Evaluation and Feasibility Study for the Need of New Dosimetric Tools and Metrics for Lung Cancer Patients Receiving Radiotherapy

by

Ahmed Omer Nawaz

A Dissertation Submitted to

Rutgers – School of Health Professions

In partial fulfillment of the Requirements for the Degree of

Doctor of Philosophy in Biomedical Informatics

December, 2018

RUTGERS
School of Health Related Professions

Final Dissertation Defense Approval Form

An evaluation and feasibility study for the need of new dosimetric tools and metrics for lung cancer patients receiving radiotherapy.

BY

Ahmed Omer Nawaz

Dissertation Committee:

Suril Gohel, PhD

Shankar Srinivasan, PhD

Frederick Coffman, PhD

Approved by the Dissertation Committee:

_____ **Date:**_____

_____ **Date:**_____

_____ **Date:**_____

INSTITUTIONAL REVIEW BOARD

The data used in this study was presented to the IRB at the Main Line health Office of Research Protections for a review on whether or not IRB approval was needed or not.

The since the data was acquired retrospectively, is anonymized, contains no HIPPAA identifiers, nor does it have any other forms of information in the data that could identify or be linked to any person(s). It was determined that no IRB approval under the Code of Federal regulation 45 CFR 46.102(f).

The author of this dissertation and the external reviewer Won Chang MD, were notified via email by the office of research protection of that no IRB approval was needed for the use of this data.

Please contact the author or the mainline heath IRB office listed below with further questions.

Office of Research Protections

259 N. Radnor Chester Road, Suite 290

Radnor, PA 19087

Phone: 610-225-6221 Fax: 610-293-8202

TABLE OF CONTENTS

ABSTRACT

Radiation oncology has made great strides forward specifically in the treatment of lung cancer. However, these advances have themselves delivered new questions that clinicians face when attempting to treat tumors in the lungs. The first of which is how to best deliver an increasing radiation dose to a small moving target. The second is how best to estimate and predict the damage to healthy lung tissue as a consequence of these higher doses.

Clinicians and academics from around the country have tabulated data, the purpose of which is to assess the risk of radiation damage to their patients during and after treatment. The consensus among these various groups is that the risk is best assessed by two or three volumetric data points. These dose indices are believed to allow clinicians to better assess toxicity endpoints in the lungs. The literature is rich with this guidance. However, that same literature search will also reveal that there is little to no data that focuses on the changes that occur in the previously mentioned evaluation metrics during respiration. The "V's" in the V5 and the V20 are incorrectly assumed constant and unchanging.

This retrospective analysis of 10 lung cancer patients shows that those clinically used metrics of evaluation that are treated as static numbers are in fact dynamic. It shows the degree to which these volumetric numbers vary from what is currently accepted. And it presents a more stable, mass-based alternative to volumetric metrics that may be more suited to assessing dose to healthy lung tissue during radiation therapy due to its stability throughout the patient's breathing cycle.

These mass-based alternative metrics are derived from each patient's own lung volume using novel techniques involving the CT Hounsfield units. Yet, through ANOVA and two sample t-tests they show statistical significance in their difference from the volume in a rate of change analysis. The mass metrics also present more stability in their rate of change via one sample t-test and also exhibit lower standard deviations in all 10 patient's breathing cycle and therefore has the potential to replace the current metrics for assessing radiation toxicity.

ACKNOWLEDGEMENTS

I would like to acknowledge my family and specifically my wonderful wife Isabelle and my daughter Sabina both of whom have been the model of understanding as I have spent many a weekend out of the house to work on my Thesis and both of whom have borne the brunt of my absence.

I would also like to thank all the faculty members and staff in the Bioinformatics department for their continuing help and patience with me as I reignited my dream towards a Ph.D. that I had abandoned close to 15 years ago.

In particular, I would like to thanks Drs. Gohel, Srinivasan, Coffman, and Chang for all their help and patience.

And lastly to both my parents, without whom I would have never become the man I am today and never had the strength to return to school and pursue a PhD in my late 30s. And lastly, I would acknowledge my Uncle Badar, without whom I would never have had to courage to come to the United States and build a life that I cherish.

DEDICATION

It would give me great pleasure to dedicate my Ph.D. dissertation to all the strong, powerful and positive women that I have been blessed to have in my life.

From birth, through infancy, childhood and finally as father myself, I have always been surrounded by wonderfully selfless women who have protected me, motivated and inspired me, guided me and stood by me regardless of circumstances. I am truly blessed.

From my Grandmother, to my mother, Shahzadi, my older sisters Ayesha and Shama, my older cousins and aunts and now my wife Isabelle, thank you all for all that you have done, and continue to for me with no expectation in return.

All of you ladies are the shining light atop a hill that I aspire to reach!

THANK YOU for all that you do and all that you are!

LIST OF FIGURES

LIST OF TABLES

LIST OF ABBREVIATIONS

3DCRT	Three-Dimensional Conformal Radiation Therapy
3DCT	Three-Dimensional Computer Topography
4DCT	Four-Dimensional Computer Topography
AAPM	American Association of Physicists in Medicine
ASTRO	American Society for Therapeutic Radiation Oncology
AvgIP	Average Intensity Projections
cGy	centiGray
CT sim	Computer Topography Treatment Simulation
D10	Dose received by 10% of the volume of interest
D20	Dose received by 20% of the volume of interest
D5	Dose received by 5% of the volume of interest
DFS	Disease Free Survival
DNA	Deoxyribonucleic Acid
DVH	Dose Volume Histogram
GTV	Gross Tumor Volume
Gy	Gray (1 Joule/Kg)
HU	Hounsfield Unit
IEC	International Electro Technical Commission
IRB	Institutional review board
IMRT	Intensity Modulated Radiotherapy
M10	Mass of Volume receiving 10Gy
M20	Mass of Volume receiving 20Gy
M5	Mass of Volume receiving 5Gy
MIP	Maximum Intensity Projection
NSCLC	Non-Small Cell Lung Cancer
OAR	Organs at Risk
PH	Breathing Phase
QUANTEC	Quantitative Analyses of Normal Tissue Effects in the Clinic
RAD	Radiation Absorbed Dose
RPM	Real-time Position Management
RTOG	Radiation Therapy Oncology Group
Rx	Prescription
SBRT	Stereotactic Body Radiosurgery
SC	Slice Collimation
SI	International System of Units (French: Système international)
SV	Seminal Vesical
T_b	Time to complete one breathing cycle
T_d	Time to complete one complete scan
TF	Table Feed
T_g	Time to complete one for CT gantry to rotate
TPS	Treatment Planning System
TRP	Treatment Related pneumonitis
V10	% or cc of volume of interest receiving 10 Gy
V20	% or cc of volume of interest receiving 20 Gy

V5	% or cc of volume of interest receiving 5 Gy
XRT	X-ray Radiotherapy

Chapter 1

INTRODUCTION

.

1.1 Objectives and Goals

The objective of this dissertation is to look at current trends and best practices in modern radiation oncology techniques in the treatment of lung cancer. Specially, to examine how the radiation oncology community evaluates and assess radiation dose delivered to healthy lung tissue during the course of treating lung tumors. These dose points calculated in healthy lung tissue are consequential as they guide clinicians on whether or not to allow a radiation treatment plan to be delivered to the patient. These dose points have been retrospectively correlated to in predicting treatment related pneumonitis (TRP) and other toxicities that compromise lung function due to radiation treatments.

The goal of this retrospective analysis is demonstrate that the currently used dose metrics may not be an accurate representation of the actual doses absorbed by the healthy lung tissue of a patient being administered radiation therapy. Then to exam if there a different methodology that can be deployed to evaluate dose to lung tissue that will not suffer from the same

1.2 Current Cancer statistics

The American Cancer Society estimates that of all the new cancers diagnosed in 2017 lung cancer accounted for 13 and 14% of all new diagnoses in men and women, respectively. Of the estimated 222,500 new cases of lung cancer, 155,870 of those patients will die from their disease. Of the tabulated data from 2017 more people would die from lung cancer than prostate, breast and colon cancer combined. It also accounts for 25 and 27% of all cancer-related deaths in women and men, respectively. It is currently the leading cause of cancer-related deaths in both men and women in the United States[1].

Cure rates for disease sites such as prostate and breast cancer are at all-time highs. The five-year survival for stage IIA prostate cancer is close to 100%, over 90% for breast cancer and 87% for colon cancer for the same stage disease. Lung cancer remains as one of the highest cause of mortality in the United States. The 5- year survival for stage IIA lung disease is still about 30%. Although improvements in survival rates for lung cancer have improved over the last decade, they are not nearly as high, nor are their rates of increase as high as other tumor sites and histology[1].

This deficit in advancement and historic lack of interest in lung cancer was thought to be a culmination a number of reasons. The first being the stigma with lung cancer being caused is a self-inflicted wound because of smoking[2]. The second is understanding the biology of a heterogeneous histological group of cancers, and also due to the anatomical challenges Oncologists face when treating a tumor in a critical organ which has high sensitivity to radiation induced damage and normal tissue field

damage resulting in chronic pulmonary disease due to putative causes such as smoking[3-5].

1.3 The role of Radiation Therapy

One of the treatment options offered to patients with lung malignances is radiation therapy. The purpose of radiation therapy is to target and destroy malignancies in the body while minimizing harm to the surrounding normal tissue. This is done by the transport of megavoltage level energy that is transferred to the tumor cells, causing single strand and double strand breaks in the targeted cell's DNA, all while sparing healthy tissue[6]. The American Society for radiation oncology (ASTRO) and the American Cancer Society estimate that of the 1.685 million newly diagnosed cases of cancer in 2017 in the United States, two-thirds of these cancer patients will receive radiation therapy at some point during their care[7].

Although there are many forms and options for radiation therapy including electron therapy, orthovoltage therapy, heavy ion and charged particle therapy, the most common form of radiation therapy consists of mega electron volt photons (MV photons). These photons can be generated using a high-energy gamma source, for example cobalt – 60 or more commonly in the United States using linear accelerators to generate X-rays.

Once the clinician has deemed the patient is a suitable candidate to receive radiation therapy, there are a series of stages that the patient must undergo before an acceptable radiation treatment plan that is specific to the patient's anatomy can be

generated. The first of these steps is referred to in radiation oncology as the simulation stage.

It is referred to as the simulation stage because the patient is immobilized on a flat carbon fiber table and then scanned via the computer tomography simulator (CT-Sim). Typically, a radiation oncology CT simulator is slightly different from the diagnostic CT machine, in that it has the larger bore and field-of-view. This is to accommodate both the patient and a variety of immobilization devices that are necessary to reproduce the patient's precise position consistently through the course of their treatment. These treatments can range from 4 to 8 weeks of radiation treatments, five days a week and more recently, highly precise treatments called stereotactic body radiotherapy (SBRT), may deliver high doses of focused radiotherapy in three to five fractions.

A three-dimensional CT (3DCT is performed to extract and extrapolate the patient's internal and external geometry upon which dose calculations can be performed. The three dimensions in a 3DCT are the standard Cartesian coordinates of X, Y, and Z. Typically, a high resolution 3DCT is more than sufficient for radiation treatment planning on most tumor locations or sites. However, on dynamic organs with tumors or tumors that are around dynamic organs, a 3D static snapshot of the patient's anatomy is insufficient for an accurate representation of absorbed dose. An example of this would be a lung tumor or esophageal cancer.

For patients that require an assessment of both a tumor and or environment in which the tumor is located a four-dimensional computer tomography (4DCT) simulator is used. A 4DCT, utilizes the first three dimensions similar to a 3DCT, that is, Cartesian coordinates X, Y, and Z, and then introduces a fourth temporal

dimension. Using an external marker on the patient's chest, the software is able to correlate the breathing phases of the patient with the movement of the marker as a function of time. This allows the software to bin specific back-projections associated with each of the breathing phases and reconstruct the patient topography for each of those phases independently.

1.4 Lung cancer histology and treatment recommendations

There are two major contributors to lung cancer. They are categorized histologically as small cell lung cancer (SCLC) and non-small cell lung cancer (NSCLC). Per the American Cancer Society[1], between 15- 20 % of all lung cancers diagnosed in the USA are SCLC and over 80% of all lung cancers are NSCLC. Of those NSCLC, approximately 40% are adenocarcinomas; between 25-30% are squamous cell carcinomas. Only between 10 -15% are large cell carcinomas.

The average 5-year survival rate of the Stage I (A1-A3) of NSCLC is 84% compared to 31% of stage I SCLC. Similarly, for stage II it is an average of 56% vs. 19% for NSCLC and SCLC respectively and for stage III it is an average of 25% vs. 8% in the same order.

The recommendation for radiation for both diseases is virtually the same per the National Comprehensive Cancer Network (NCCN) guideline from radiation doses for both NSCLC and SCLC. The recommendation for treatment for both histology is the same dose range of between 60-70Gy for the standard dose fractionation. So no matter which diseases the patients had, they would essentially get the same dose under the standard of care for lung cancer.

In the study the focus is on tools used to assess the risk to health lung tissue as a consequence of radiation treatments rather and tumor response. More specifically, it is on the "low" dose region of ~50% or less of the prescribed radiation dose that affects healthy lung but not the tumors. So whether or not the disease treated is SCLC or NSCLC would have no impact on the data.

1.5 Use of four dimensional CT simulators

The use of 4D CT simulators has become more commonplace across clinics in the United States, however, their uses are primarily focused on tumor localization and tracking. To this end, most centers will use a 4D CT of the patient to generate both a maximum intensity projection (MIP) CT scan and an average intensity projection (avgIP). The MIP will be used to identify and delineate the target and the avgIP would be used to compute the radiation absorbed dose treatment plan. This analysis will expand the use of the four-dimensional treatment plan to more just tumor localization and dose computation. It will effectively uses that very same data set to the extraction meaningful data from a 4DCT in the form of volumetric changes in the lung during all phases of the breathing cycle in addition of changes in the dose points during the breathing cycle.

This analysis intends to address the challenges of computing radiation dose in a moving target with various changes of density along a radiation beam path leading to different rates of absorption. The secondly, to try and understand how these density changes and movements affect patient treatment plans and their evaluation. Lastly, the

challenge is to devise a new and meaningful strategy to try and address these changes. The use of 4DCTs will be instrumental in assisting in addressing these challenges.

1.6 Radiation treatment planning for lung cancer

One of the primary toxicity endpoints during radiotherapy is radiation-induced pneumonitis[8,9]. The goal of all radiation treatments for lung cancer is to deliver the maximum amount of dose to the tumor while sparing as much of healthy lung tissue as possible. The goal is to achieve this objective without compromising the prescription dose to the target. Although radiation-induced pneumonitis is expected in the targeted region of the lung, there been several studies that have shown this toxicity may occur outside the radiation field or near it. Also, fatal pneumonitis is possible when adjuvant therapy such as extra-pleural pneumonectomy and adjuvant chemotherapy[10] are used together with radiation therapy. To this end, there are recommended dose limits that are allowed during radiation treatment to healthy lung tissue in order to maximize the dose to the tumor volume and minimize the risk of damaging the excessive amount of healthy lung tissue as a consequence of treatment[11]. There used to be a single metric for the healthy lung tissue which was that the volume of the healthy lung, that is the lung minus the gross tumor volume(GTV) receiving 20 Gray (Gy is SI units for radiation absorbed dose units; 100RADs =1Gy) should be below 30%[12]. For reference, the typically prescribed radiation dose for lung cancer varies between 56 and 66 Gy, depending on the stage and location in the lung. In more recent publications that constraint has been tightening and now asks for the V20 to be below 20% and in addition has added a lower dose metric of the V5 to be

below 65%. This lower dose metric of the total lung dose receiving just 5Gy is a function of studies showing that the low dose regions are also good predictors of potential radiation-induced pneumonitis outside the treatment area. For reference, similar constraints exist for other tumor sites such as prostate and breast cancer.

1.7 Adverse effects of Radiation

There are two ways in which biological tissue responds to high levels of ionizing radiation. The first is acute or early effects and the latter being chronic or late effects. Acute effects can be seen in tissues within a month or less of the patient's completion of therapy. Late effects can manifest within a few months or sometimes several years after treatment has been completed. Tissues that undergo rapid divisions such as the endothelial cells in the gut and mucous membranes are acutely sensitive to radiation, as discussed earlier since radiation very rarely kills the cell, rather it inhibits the cell's ability to further divide.

Radiation dose tolerance also has to do with cell proliferation and mitotic divisions. Tissues such as nerves and muscles are extremely radio resistant due to the fact that the cells do not divide. Tissues such as the oral mucosa, endothelial cells and testis have rapid cell productions and are generally the first two exhibit effects of radiation[6].

For the study, we are examining the lung region, and lungs due to their radiobiological profile suffer from acute effects, such as treatment related pneumonitis (TRP). The tumors that are treated in the lung vary in their response to radiation. Tumor histology and origin contributes to this uncertainty.

1.8 Problem with current dose limits methodologies used in lung cancer therapy evaluation.

The shortcoming of the dose constraint methodologies currently used, as referred to in previous section when applied to the lungs are, that these constraints are a function of the overall and total volume percent of the lungs. During treatment for disease sites such as prostate and breast cancer, the volume of the tumor and proximal organs at risk stays constant through radiation treatment. The lungs, however, are dynamic organs and constantly change their volume during the delivery of radiotherapy.

These evaluation metrics involve performing a three-dimensional analysis of the entire organ and a volume normalized histogram is created referred to as a dose volume histogram or DVH. The purpose of normalization is so that multiple organs and tumor sites can be visualized on the same histogram with absolute dose. Although, the first published uses of a DVH was in 1985[13] and used to assess liver dose, it was first used to assess lung dose in 1991[14] in a comparative study to assess the difference between two different planning techniques.

In figure 1.1, is an example of a DVH of initial phase of radiation dose being delivered to a prostate plus seminal vesicles target. The three organs at risk in the male pelvis near the prostate are the rectum, the bladder, and the femoral heads. Since they are all different volumes it would have been difficult to visualize them on the same histogram without normalizing the volume of all the targets and Organs at Risk (OARs).

The DVH model of assessing dose tolerances for organs at risk has proven invaluable in the continued effort to increase the dose to the tumor target. The reason being one of the factors that limit the amount of dose that can be delivered to the tumors is the toxicity to surrounding OARs. The more we can understand their response and create techniques for sparing them, the higher the chances that the patient has of a tumor response

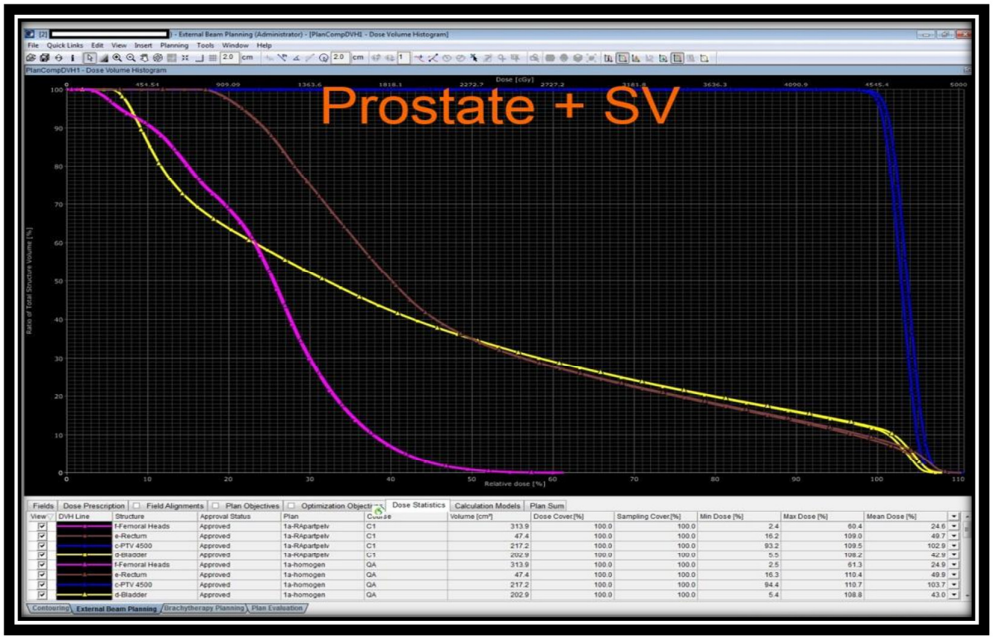

Figure 1.1 *Sample DVH that plots and shows the organs at risk i.e. the femoral heads (pink), the bladder (yellow), the rectum (brown) and the targets (blue).*

.

Unfortunately, for historical reasons the same DVH models are used to evaluate lung tissues with the primary assumption being that the normalized volume this stagnant and unchanging during treatment as it is for the rectum and bladder during prostate irradiation. Although known to be false, clinicians and medical physicists continue to use this tool because it is the only one that they have at their disposal.

1.9 Significance and Novelty of this study

There has been a large and concerted effort on the part of the entire radiation oncology community, since the commercial availability of 4DCT in radiation oncology clinics. The quick search of the literature over the past 20 years reveals that the primary focus of the academic community has been on tumor localization and targeting. The philosophy and reasoning behind this methodology is consistent with the challenges that radiation oncologists and medical physicists were facing at the turn-of-the-century. The observance of increasingly high failure rates and abysmal survival for lung cancer patients versus other tumor histologies was generally attributed to the primary issue which was the uncertainty of the tumor volume or target inside the lung.

Due to the known uncertainty in tumor volume delineation in the long treatment methodologies included a drastic expansion of the radiation field size and treatment area. This led to a significant limit to dose escalation. When compared to other adenocarcinomas such as prostate cancer, whose prescription started in the early 2000's at around 60-65Gy are now being treated for the same disease with 80-85Gy. The general prescription for non-small cell lung cancer remained at around 60Gy for the better part of the last two decades. With 4DCT technology and enhanced understanding of tumor motion and localization is not uncommon now to see lung tumors being treated to 66Gy. This dose escalation has been limited also by the surrounding OARs (healthy lung tissue). Which is why most of the literature on this technology focuses on targeting and chasing tumor volumes. Once Pan *et al*. [15]showed

that target delineation was possible dose escalation began with higher dose in conventional radiation and SBRT.

With all this focus on lung cancer targets there has not been a lot of literature about how this 4DCT technology can be better used to assess the dose to the healthy lung tissue. As will be shown in section 3.5.3 in chapter 3, most treatment protocol can recommendation still reference the volumetric data point as limits to healthy lung dose tolerance. This study will show that those tolerances recommended in the literature move in measurable way and that defining them as a static dose point is problematic.

A PubMed search with the key words *lung, dose* and *mass* yields a single paper with relevance from 2018 titled "*Real-time energy/mass transfer mapping for online 4D dose reconstruction*"[16]. Even in this paper, the focus is on errors in the primary target (internal target volume or ITV) and the expansion of that target to account for uncertainty (Planning Treatment Volume or PTV). The percent error were reported as 11.3% and 4.4% respectively.

Even with variation of search parameters to change *dose* to *radiation* etc. the PubMed results in this topic primarily reveal papers that focus on the tumor volumes and the effect that breathing during treatment has to the tumor dose and then the use of 4DCT technology to assess the errors. When *dose* and *mass* are used the paper by Watkins *et al.*[17] can be found published in Oct of last year. In this paper the authors' again focus on the use of dose to mass histogram as the means to optimize the PTV of 10 patients. They do, however explore the variation in the dose to mass vs. dose to volume of lung, but they do not explore how the temporal effect of the breathing has on the variation of the dose to mass vs. the dose to volume as this study explores.

After a more exhaustive search via other methods including Google Scholar, there are a few other posters and abstracts that can be found on the subject similar to the concepts that this thesis explores. A poster presentation from the Virginia Commonwealth University (VCU) group that published the previously mentioned paper on dose mass optimization in which the poster evaluates dose mapping errors in 4DCT[18]. A poster presentation from the Fox Chase group, in which the concept of the dose mass histogram is explored[19] is worth noting as well. However, it is worth mentioning that the Fox Chase group presented this abstract to the annual AAPM in 2016, but the author of this thesis Nawaz *et al.* first explored this concept in a poster presented to AAPM in 2015[20].

Chapter 2

PRICIPLES OF METHODS USED IN GENERATION OF PATIENT SPECIFIC 4DCT DATA

2.1 Challenges and need for precision.

As with all workflows clinical and nonclinical, an early error or inconsistency introduced to the workflows propagates downward through the rest of the process. Similarly, in radiation therapy treatment planning the need for accuracy in the initial simulation is crucial to the accuracy of all proceeding steps, including treatment planning, optimization, tumor localization and treatment delivery.

The demands for precision 4DCT acquisitions are very high due to the additional temporal component of the scan. If the patient data set were not to be acquired in high temporal and spatial resolution there is a danger of inaccurate identification of the target track or tumor motion. This error would then propagate to the workflow ultimately resulting in a suboptimal result for the patient.

2.2 Basic principles of CT acquisition

Before understanding the complexity that the temporal component of a 3DCT scan introduces, it is first important to understand the challenges of image acquisition in a static 3DCT. This is important as the most all radiation therapy 3D dose

distributions are calculated on a 3D Volume. The crucial component of a good 3DCT data set is for the scan to be high resolution, specifically, have high spatial resolution.

Once on a CT table, the patient is scanned from a variety of angles (Φ) and back projections of stacked images are then used to sample the attenuations of those projections (P_{ϕ}^{CT}). Since the primary source in a CT is a polychromatic spectrum, the detectors are able to sample the intensity (*I)* and then the software is able to integrate all the initial measurement I_0(E*)* while taking into consideration, the entire energy spectrum (0 … E_{max}*)*.

Then with Lambert Beer's law of attenuation allows for measurement of intensity to be given as:

$$I = \int_0^{E_{max}} I(E)dE = \mathrm{I}_0 \,. \int_0^{E_{max}} S(E)\, e^{-\int_0^1 \mu(E,\vec{x})d\vec{x}}\, dE \qquad (2.1)$$

where μ is the total mass attenuation coefficient and the $S(E)\, e^{-\int_0^1 \mu(E,\vec{x})d\vec{x}}$ is change in spectral energy for greater depths. Due to the disabling affect that the strong energy dependence has on spatial distribution, it will not allow for the determination of the spatial distribution of μ along the trace *l*, therefore the assumption of an average energy of *E* is required.

$$\int_0^{E_{max}} S(E)\ dE = 1 \qquad (2.2)$$

And allow for the profile P_{ϕ}^{CT} to expressed as

$$(P_{\phi}^{CT}) = -\mathrm{In}(\frac{I}{I_0}) = \int_0^1 \mu(E,\vec{x})d\vec{x} \qquad (2.3)$$

This allows for $\mu(x, y)$ to be reconstructed as a planar object, as the projection of the object from a particular set of angles Φ is acquired. The intensity profiles were measured from a multitude of angles across the η direction. This is done so that the coordinate of the object along the trace ξ can be used to cover the entire object in that slice.

This induces a new set of fixed coordinates in the two dimensions of x and y. These can be used to show how μ is distributed inside the object with respect to a fixed coordinate system. The angle Φ and coordinates η and ξ can be used to define x and y:

$$x = \xi \cos(\Phi) - \eta \sin(\Phi) \tag{2.4}$$

$$y = \xi \sin(\Phi) + \eta \cos(\Phi) \tag{2.5}$$

Equations 2.4 and 2.5 allow for the definition of η in relation to x and y and the angle of projections Φ. ξ is negligible and therefore η depends on Φ, x, y is defined as:

$$\eta(\Phi, x, y) = \frac{y - x \cdot \tan(\Phi)}{\tan(\Phi).\sin(\Phi)+\cos(\Phi)} \tag{2.6}$$

This allow for $\mu(x, y)$ to be described with a series of projections. And where a with a single measurement:

$$p^{CT}(\Phi, \eta) = -\ln\left(\frac{I(\Phi,\eta)}{I_0(\Phi,\eta)}\right) = \int \mu(\bar{E}, x, y)dl \tag{2.7}$$

So, based on measurements of $p^{CT}(\Phi, \eta)$ an object $\mu(x, y)$ can be reconstructed into a CT. This can be expressed as the Radon-Transformation(**R**) and allows for the two-dimensional function of $\mu(x, y)$ with all 1D projections expressed in $p^{CT}(\Phi, \eta)$ to be expressed as

$$p^{CT}(\Phi, \eta) = \mathbf{R}[\mu(x, y)] \tag{2.8}$$

And then the expression of the inverse Radon-Transformation (R^{-1}) to describe $\mu(x, y)$. This yields the trivial back-projection ***B;***

$$\mu_{\boldsymbol{B}}(x, y) = \mathbf{B}[\, p^{CT}(\Phi, \eta)] = \mathbf{BR}\,[\mu(x, y)] = \int_0^{\pi} p^{CT}\left(\Phi, \eta(\Phi, x, y)\right) d\Phi \qquad (2.9)$$

The acquired back-projection in (x, y) are the result of the integration of the projections p^{CT} that trace through the system coordinate (x, y). These projections are acquired from 0^o to 180^o for the sake of symmetry. One of the pit falls of this is that the system assumes that the resulting back projection is not a precise definition of μ, as the method assumes that all to the of the coordinates acquired are found along the two-dimensional projection line, even though it is known that some of them will be at a distance from (x, y). The result value of $\mu(x, y)$ is then falsified. Also, the product of the **B*R** results in a convolution of $\mu(x, y)$ with the kernel $h(x, y) = |\,(x, y)|^{-1}$, where $h(x, y)$ is the point spread function (PSF).

$$\mathbf{BR}\,[\mu(x, y)] = (\mu * h)(x, y) \qquad (2.10)$$

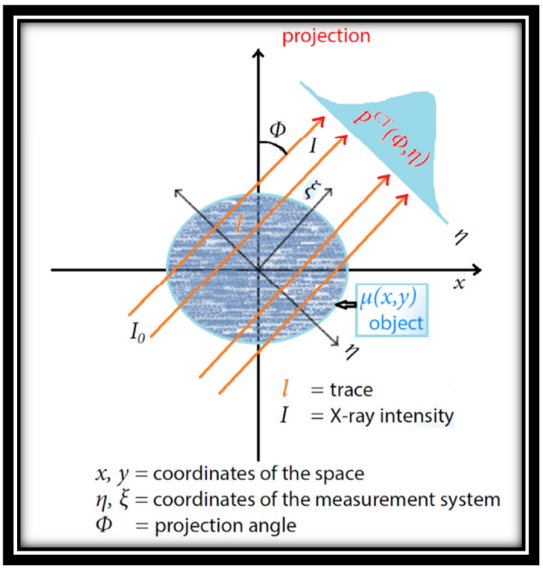

Figure 2.1 *CT back projection aquisition*

Then the achieved back-projection of a single Dirac signal $\delta(x, y)$ gives $h(x, y)$. This also shows the importance of the trying to reduce the $1/|\vec{r}|$ sloping. Therefore, to define μ the objective is to try and remover the PSF from back-projection $\boldsymbol{B}$. This is done via a filter function, prior to the back-projection. The convolution of $pCT\,(\Phi, \eta)$ signal with h^{-1} kernel is referred to as a filtered back projection. The Radon-transformation is defined as:

$$\mu(x, y) = \mathbf{B}[(p^{CT} * h^{-1})(x, y)] \tag{2.11}$$

2.3 Hounsfield Units

When the attenuation coefficients ($\mu_{CT} = \mu(\bar{E}, x, y)$) through an object is reconstructed via computer topography, there is a need for a format that is relative and that can be scaled easily. The Hounsfield-Units (HU) is that scale[21]. The values on an

HU scale are defined relative to the attenuation of water $\mu CT\,(H2\,O)$. This allow for a dimensionless and unitless value defined by the equation 2.12:

$$\text{HU} = \frac{\mu CT - \mu CT\,(H2\,O)}{\mu CT\,(H2\,O)} * 1000 \qquad (2.12)$$

By the equation above it this clear that the HU is a scale in which tissue density is defined as a ratio of that tissue to water in the thousandth. Although the scale can go from $-1000 \leq \text{HU} \leq \infty$, where -1000 is the HU for air and 0 HU is for pure distilled water, it is well known that tissue very rarely exceeds 2000 HU. Most clinically used HU scales go up to ~12000 to accommodate for artificial implants such is dental filling, titanium knee and hip replacements etc. These numbers are then illustrated to the user in grayscale. This allows for window and level of the subsequent reconstructed image so that a certain range of HU are more or less prominent by making certain pixels "more white" or more dark.

The user can also limit or define the range of pixels that can be seen. This allows for a contrast in the image to appear making it easier to see different parts of the anatomy[22-24] as seen in figure 2.1. It's clear from these figures that using various filters of the Hounsfield units the same image can be used to better visualize different parts of the patient's anatomy. Figure 2.2 show the same slice of the patient's cross-sectional anatomy. Panels A through D demonstrate preset window and level settings. Panel A is set so that the bones of the patient are best visible to the viewer, however it is clear that the soft tissue inside the skull is not very defined. In contrast to that, panel C is set to best visualize the brain. Although it is the same CT set, with the same information on the same slice it becomes clear that both the brainstem and ventricles are easier to visualize however, the high signal from the C-spine makes it difficult to visualize each vertebral body as clearly as was possible in panel A. Panel B and D are

different window level settings that are more commonly used in the abdomen and thorax region but are displayed as a visual representation of how adjusting the Hounsfield units can change the appearance of a CT scan.

2.4 Relevance of CT density calibration curve in Treatment planner

Besides the visual advantages of Hounsfield units, the modern radiation treatment planning system (TPS) also uses these numbers as an interpretation of density. This is referred to as a heterogeneity correction in computing radiation dose path length[25]. An example of a CT to density curve can be seen in figure 2.2 and how the same CT image can be made to present different information. A Bone: Window 2500 HU ; Level 50HNU, B Lung : Window 1324 HU; Level -362 HU, C Brain : Window 80 HU; Level 40 HU, D Soft tissue : Window 500 HU; Level 39 HU. In fact, this is the CT curve upon which are the treatment plans calculated for the study were computed. The measured values in this curve were taken from a phantom with various known density plugs.

This phantom was then put in the clinical CT scanner and the average Hounsfield units for each plug were tabulated and entered on the CT curve. Although it is acceptable to use published funds for the unit data for known densities, the AAPM recommends that each clinical CT scanner be assigned its own unique CT to density curve, this is because there are slight variations from one CT scanner to the next.

It is also clear that the CT to density curve is not linear. However, for the purposes of this study, we are looking at lung densities in the order of 0.3 gm/cc, that portion of the curve is linear

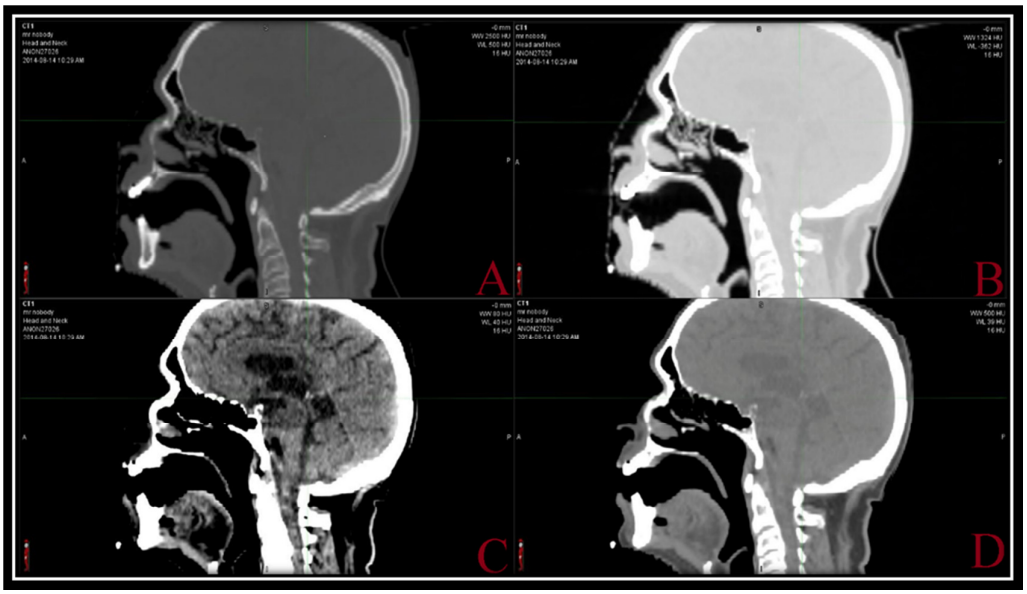

Figure 2. 2 *Sample CT cut of the same patient at the same location displayed with different window and level.*

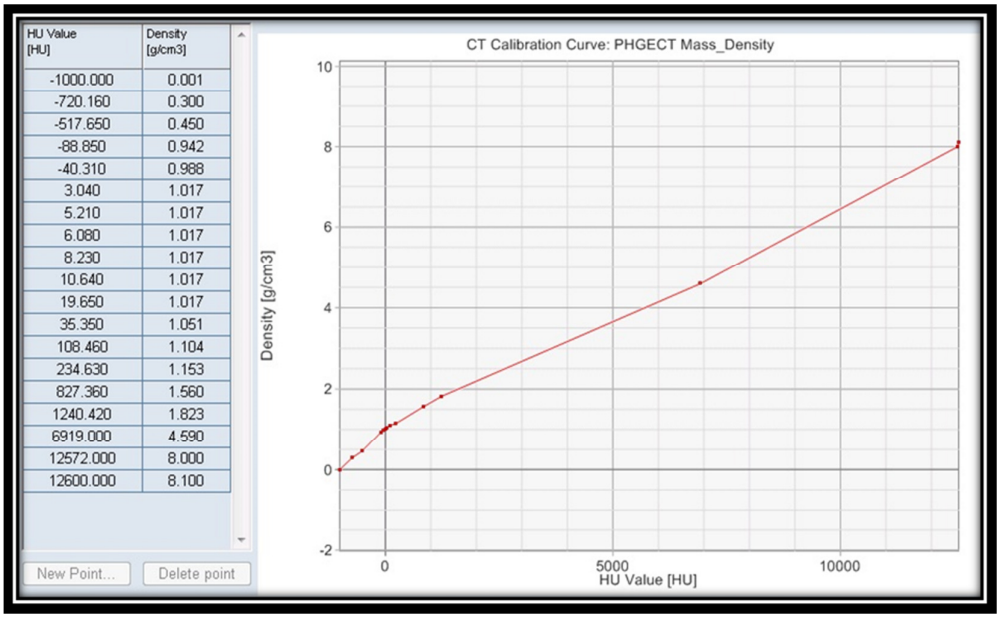

Figure 2.3 *CT to density curve used by treatment planning systems*

Most all modern radiation treatment planning systems (TPS) require inputted data dose measured on the linear accelerator that is being modeled. These measurements are all done by physicists and are all done inside water. With water being the gold standard of radiation absorbed dose, TPS have a benchmark of density across which the radiation absorbed and deposited along the particular beam path can be set. For example, for a six Mega Electron Volt photon energy that is delivered to a flat water surface, 10 cm depth in that water is expected to get the 66-68% of the initial dose. Now if the treatment planner what to compute the same beam path but in lung tissue rather than water more dose would be expected at the 10 cm depth. This is because lung tissue is approximately 70% less dense than water, therefore less of the dose would be absorbed by the tissue along the 10 cm travel through the tissue, resulting in more dose to the point where the measurement is taken[26]. This concept of radiological path length is described in greater detail in the preceding section 2.9.4.

2.5 Motion artifact with 3DCT imaging

One of the concerns related with a 3DCT of dynamic organs such as lung and other organs close to the diaphragm is motion artifact. These errors have been well document and the preceding figure below illustrate one of the primary reconstruction error in 3DCT of the diaphragm[27]. As can be seen in figure 2.4 on the left. The oval shape is up and down representing the inhale and exhale direction, as indicated by the green arrows. At the same time, it is being scanned on a CT table from positions 1 through 3, the way in which the image would be reconstructed would lead to an imaging artifact. This would result in a serious misrepresentation of the size and shape

of the oval. The image on the right of figure 2.4, is the physical manifestation of this artifact. As is clear, the diaphragm has not been accurately reconstructed and is lending itself to the artifact shown in the image to the left of it.

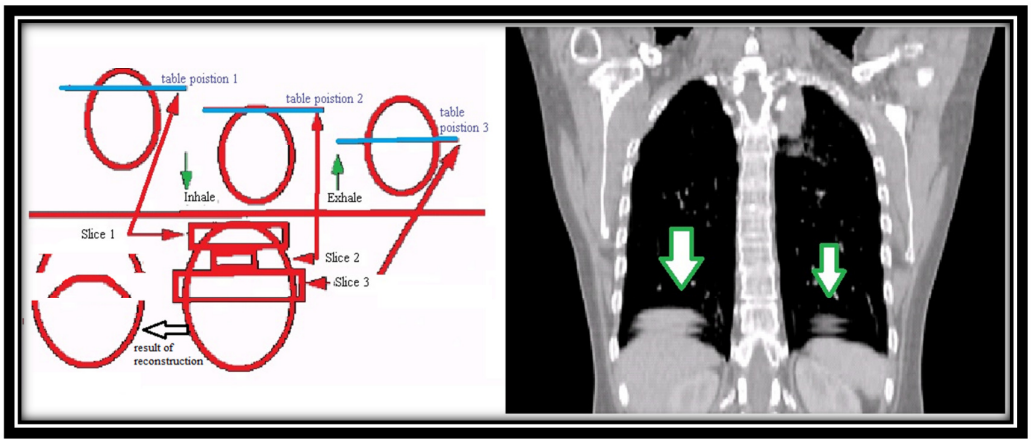

Figure 2.4 *CT reconstruction errors for a dynamic target and how those reconstruction errors can manifest shown on the image to the right.(The figure on the left was taken from Balter et al.*[27] *and modified by the author of this thesis)*

The challenge that these artifacts present is that the volumetric data is unreliable. More critical than that, if this artifact were to present itself over the tumor site, it could lead to a gross underestimation of the target and have disastrous consequence for the patient's chance of disease free survival (DFS). To address this radiation oncologists would use very generous margins around the identified target and would run the risk of treating potential healthy lung tissue to mitigate the chances of missing the tumor. Some older protocols would call for planning margins around the tumor volume to be up to 2 to 3 cm to account for tumor localization and uncertainty and patient set up variations[28]. What this meant was if there was a tumor with a 1 cm diameter that would equal a total of 3.14 cm^3 of volume that needs to be treated. Adding a 3 cm margin would increase that treated area to 28.27 cm^3, resulting in nine-fold increase of the treated area. Some of these issues were addressed when 4DCT became more available, as is discussed in the next section.

2.6 - 4DCT and the requirement for dynamic temporal imaging

With the first implementation of 4DCT in the early 2000's lung tumors[29] that were particularly susceptible to over or under radiation were now in the spotlight. A 4DCT is a four-dimensional computer-assisted topography of the patient's anatomy. As mentioned earlier, this is achieved with the first three dimensions being the spatial coordinates and the fourth dimension being time.

Acquiring and collecting data from a 4DCT is an attempt to reconstruct a part of the patient anatomy that is periodically deforming. There are several criteria that have to be met before a clinically significant data set can be extracted[15,30]. The first of which is the scanning time T_d. That is, the time required to complete one scan, must be less that T_b, the time it takes for one full cycle of the motion to complete. In the case of human anatomy, T_b would be one full breathing cycle. We know from equation 2.9 that only half a rotation is required to reconstruct one CT slice, so Tg would be defined that the time required to for that those back projections to be acquired.

A typical patient's breathing cycle can range from $3s \leq T_b \leq 6s$ and the typical Tg for a CT gantry is around 0.5s. This Tg is more than sufficient for the acquisition of a 4DCT data set. It will also allow for the acquisition of four slices per second and yield a temporal resolution of 0.25 seconds. This fast scanning and real-time CT reconstruction is required for larger organ such as the lung which in an average adult

can be from 13-16 centimeters long[31]. In the CT scanner that acquires images using helical multislice imaging, the pitch is also important. The pitch factor of the CT is limited by the maximum T_b. This pitch is defined by the International Electrotechnical Commission (IEC) as:

$$P = \frac{TF[mm]}{N.SC[mm]} \tag{2.13}$$

Were *TF* is the "table feed" and is a measurement in millimeters of the CT table moving per rotation in time T_g, N is the value of the detectors array and *SC* is the slice collimation. If *P* were equal to 1 then the scanner would acquire one beam collimation per rotation. The speed at which the images are processed is determined by the pitch. This then leads to the maximum allowable period time T_b, to be defined as:

$$T_b \leq \frac{N-1}{N} \cdot \frac{Tg}{P} \tag{2.14}$$

Where (*N*-1)/*N* is the factor that is used to correct for a CT scan that has the ability to scan multiple slices simultaneously. It is worth noting that almost all modern radiation oncology centers have a multislice CT scanner. These scanners also require that when acquiring CT slices there be an overlap from one section to the other. As discussed earlier the ratio between the rotational time T_g and the pitch *P* is a description of the temporal coverage. What that would mean practically would be that, in a 16 slice CT scan, if a patient has a breathing period of T_b = 5seconds, to get a meaningful 4DCT data set the scanner would have to have a *Tg* = 0.5s and a P = 0.1[32]. As will be seen in Section 2.8, 4DCT are error prone due to a variety of reasons the incorrect pitch and gantry rotation speed is one of those that contributed to these errors[33].

2.7- 4DCT image reconstruction

Reconstruction of temporally indexed CT data sets has been well described[34,35]. For the purpose of illustrating the errors that occur when reconstructing a respiratory correlated CT set this topic will briefly be discussed for both helical rotation and cine mode. Cine mode refers to data acquisition with the table feed in a step-by-step motion whereas helical CT sets are acquired with the table feed in continuous motion. Helical mode is also sometimes referred to as a spiral CT. The data acquired for this study was done in Cine mode. The general idea of reconstruction is using the CT imager and gantry to rotate around each table step position to acquire or oversample images along the patient's axis. This is done while simultaneously indexing each acquired back projection with the patient's respiratory cycle. A model of that respiratory cycle is also continuously acquired by placing an external marker on the patient's chest. This marker is then monitored via software and the motion is interpreted as a representation of the patient's breathing cycle (figure 2.6). This results in a large series of unsorted data sets that is retrospectively indexed to the breathing trace and then binned with specific breathing phases according to user preference. Although there are a variety of vendors that offer the service to radiation oncology clinics, the system that was used in this case study is the RPM system managed by Varian medical systems. In the case of this study a GE healthcare CT scanner was used in conjunction with the Varian RPM system. The system set up can be seen in figure 2.5. Clockwise from the top left: GE CT scanner with carbon fiber flat table:

infrared camera mounted to the foot of the table to monitor patient breathing: external marker with fluorescent dots placed on patient's chest: GE advantage workstation for 4DCT reconstruction: Varian RPM system monitoring movement of external marker on the patient's chest and correlating it with acquired CT images.

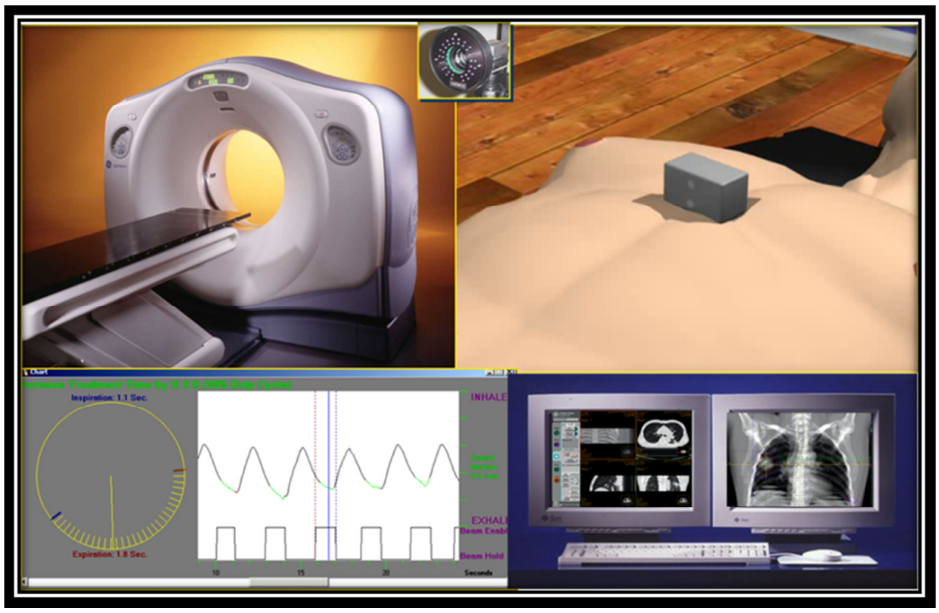

Figure 2.5 *The GE healthcare CT scanner and Varian RPM 4DCT respiratory management system.*

The hardware involved in acquiring a 4DCT consists of the CT scanner, an external marker placed on the patient's chest, an infrared camera that monitors the fluorescent markings on the external marker. The software includes the RPM respiratory management system that correlates the respiratory cycle with the acquired back projections from the CT scanner at any given time during the scan. Both the breathing trace and bulk CT back projections are then transferred to the GE advantage workstation where the user can determine the number of respiratory cycles needed (this number is typically 10 bins, 0% to 90% breathing phases).

This workstation then bins the acquired images as a function of where on the breathing phase there were acquired and reconstructs the desired number of CTs. For example, if the standard number of 10 is requested, 10 different CTs will be generated and labeled phases 0% through 90%. Once this is done, further image manipulation can occur. Physicians typically prefer to identify their target on a maximum intensity projection (MIP) scan, this is a scan where the highest signal or HU form each scan is taken and added to a single scan.

This MIP is typically used for target delineation as it takes into account the highest signal where the tumor would have been located at any point in any of the phases. One other scan that is created is referred to as the average intensity projection (avgIP). As the name suggests this is a single scan that averages the Hounsfield units of all 10 phases to produce a single CT set. This is the CT set that radiation treatment planning typically occurs on. As it is a good representation of the average position an average density of the lung tissue across which the radiation dose is computed.

It is worth noting that there are other commercially available products that include abdominal belt compression. This device uses the expansion and contraction of the belt wrapped around the patient's chest to interpret their breathing phase. One such device it is marketed and sold by Philips medical systems that work exclusively on Philips CT scanners.

The system must be able to synchronize the patient's breathing increase or waveform with both the couch positions and the acquired CT images. The standard and generally used number of bins is 10. For the purpose of this study on external marker was placed on the chest to monitor breathing

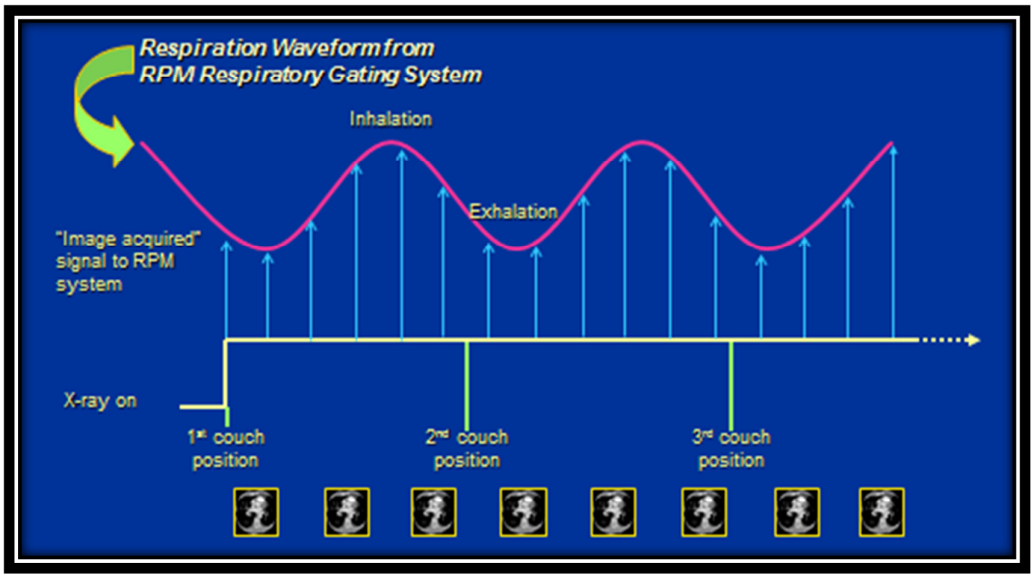

Figure 2.6 *Varian RPM system respiratory waveform correlates with the CT in a 4D image reconstruction process.*

2.8 4DCT reconstruction errors

The reliability and integrity of the reconstructed 4DCT images is crucial for accurate dose calculation. However, due to the additional complications added due to the temporal component, 4DCT imaging is more prone to errors than a standard static 3DCT. As Keall *et al.*[36]showed in a survey of the most common errors during the 4DCT, irregular breathing was the most common by a large margin. Irregular breathing accounted for 85% of the errors reported. The second most common error was reports of poor or incomplete data from their respiratory monitoring system, be it external marker or compression belt. That error rate was reported at 8%. But even though the artifacts and errors from irregular breathing are at such a high rate they cannot be excluded because irregular breathing in the patient implies a systematic error.

Pan *et al.*[15] details this some of the other potential errors and these consequences in the incorrect pitch or gantry rotation time. In figure 2.7 demonstrate the consequence of when a sphere of known 3 cm radius sphere, with a sinusoidal motion 1 cm amplitude in the cranial-caudal direction, period 4 sec and scan speed 0.2 sec and the images are reconstructed Phases 0-2p in p/4 steps. As discussed in section 2.6 and 2.7 the all of these are critical toward the effort to reconstruct a dynamic organ accurately.

What this figure shows and demonstrates is the artifact that was observed in the 3D reconstruction of a standard CT scan demonstrated by the image in figure 2.4, can also come into play in four dimensional CT scans if the period of the CT scanner is not accurate to the breathing phase. The Sphere reconstruction in figure 2.7 shows different phases demonstrates the potential error in 4DCT image reconstruction. (*It is worth noting that the details of image acquisition are detailed in the referenced paper however, these images were not taken directly from the paper that is referenced. Rather from a PowerPoint talk given by Chen et al.*[15] makes clear is how critical the setting of correct period is to resolve the correct tumor shape and size. This has the potential to lead to a serious under treatment by misidentifying and alleviating the incorrect shape of the tumor volume.

The standard way that medical physicists address the systematic error is via patient training prior to the acquisition of the CT scan. Patients are coached to breathe as rhythmically and evenly as possible. This coaching is sometimes done with the assistance of both visual and audio aids in the case of the Varian RPM system.

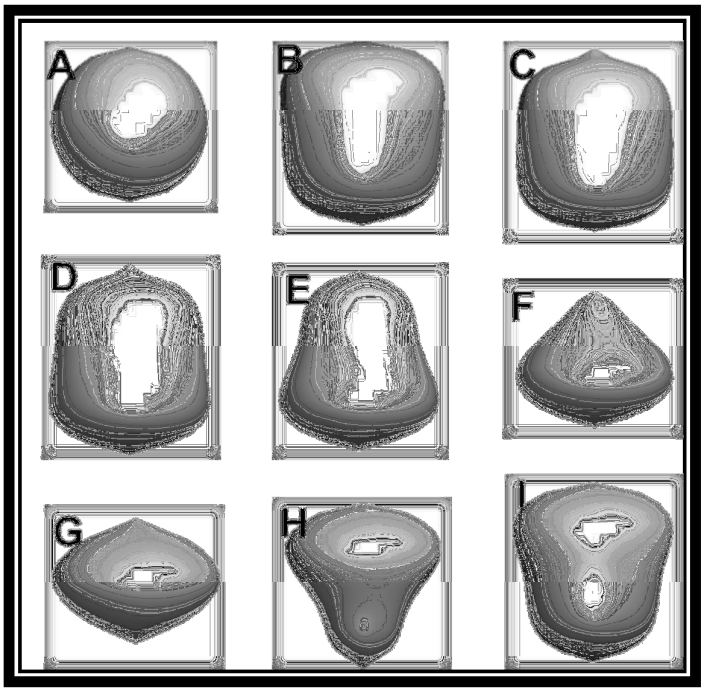

Figure 2.7 *A 3 cm radius sphere, with sinusoidal motion 1 cm amplitude in the cranial-caudal direction, period 4 sec and scan speed 0.2 sec and the images are reconstructed Phases 0-2p in p/4 steps.*

2.9 Basics of Radiation physics and treatment planning delivery.

For a better understanding of the data, the relevance of how the data is acquired and why, a brief overview of radiobiology, the basics of radiation physics and treatment planning is necessary.

2.9.1 Basics of Radiobiology

The primary purpose of clinical radiotherapy is in the hope that the ionizing radiation in the mega electron volt energy region will destroy cancer cells. Although

there is some debate in the community about the exact mechanism of cell death once exposed to ionizing radiation, the common consensus is that the radiation either performs a single-stranded or double-stranded break in the nuclear DNA leading to the inability of the cell to replicate.

The ethos of treating through healthy tissue with ionizing radiation is based on the advantage of healthy cells ability to repair damage to the DNA more effectively then malignancies. If the cancer cell's repair mechanism of its DNA, which includes checking DNA integrity, were functioning properly, when the cell detected an irreparable abnormality in its DNA that caused it to be malignant it would have triggered an apoptotic event. Apoptosis is commonly referred to as programmed cell death. In an average adult, apoptosis is a very common occurrence. Each day approximately 60 billion cells initiate apoptotic events in themselves and initiate the process of programmed cell death.[37,38]

For the reasons stated above when the radiation doses prescribed not all of it is delivered at once. The treatment delivered over the course of sevrial weeks and is refered to as fractionated. This break of total high dose over time allows the healthy tissue, through which the radiation travels, a chance to repair itself. For example, the patients in the study have received a variety of different dose schemas depending on their tumors histology and responses, some have received 66Gy in 33 fractions, some have received 60Gy and 30 fractions and finally some have even received 10Gy in 5 fractions. These choices of total dose and fractionation scheme has to do with radiobiological responses of the tumors to specific doses but go beyond the scope of this research effort. More information about radiobiology and cancer cell survival curves can be found in Hall *et al's Radiobiology for the radiologist* [6].

2.9.2 Basic Physics

There are many forms of particle therapy that are used for radiation treatment. The most common in the United States is x-ray radiotherapy. X-ray therapy involves highly any energetic photon is generated via accelerating electrons in a linear accelerator and colliding them with the target. A photon is essence is a specific quatna or bundle of energy *E* as defined by

$$E = hv \tag{2.15}$$

Where *h* is Planck's constant defined as 6.62 x 10^{-34} Joules-Seconds and *v* is frequency of the photon. There are many forms of interactions of the photons with biological matter, but in the energy range of radiotherapy, the photoelectric effect, the Compton scattering affect and pair production, are the most common particle interactions, with the Compton scattering as the primary of all three interactions[26]. The goal of physics in medicine is to bridge the gap between mechanically produced x-ray particles in a linear accelerator and convert them into absorbed dose in biological tissue. As will be discussed in upcoming chapters in more detail, that absorbed dose is has an SI unit of Gy (Gray):

$$Gray = \frac{Joules}{Kilogram} \tag{2.16}$$

2.9.4 Planning of radiation fields

Planning and delivery of radiation treatment plans in the contemporary setting is a multidisciplinary team effort. This team consists of but is not limited to the physician radiation oncologist, medical physicists, dosimetrists and radiation therapists. All of these team members have their own roles to play in the simulation

planning and treatment delivery aspects for patients to successfully complete their radiation therapy course.

The treatment planning effort is collaboration between radiation oncology physicians, medical physicists and dosimetrist. The first includes target delineation by the physician followed by identification of the organs at risk by any of the team members that have received proper training. The next step is accurate beam arrangement that's considers entrance and exit effects on healthy tissue. This results in a complicated beam arrangement followed by dose calculations.

There are several commercial radiation computational algorithms. Nearly all of them now take tissue density heterogeneity into account while computing dose. This tissue density heterogeneity is most often dealt with by adjusting the radiological path length of the beam. The simplest algorithm to understand this concept would be the ray tracing method. Figure 2.8 demonstrates a particle trajectory across six different voxels of varying density. These densities are labeled ρ1 through ρ6.

It is important to mention that the benchmark for radiological path length traversing through matter is done in water. The adjustment of the path length is also done with reference to water. Sometimes the nomenclature of radiological path length can be replaced with "water equivalent depth", i.e. depth of tissue that the beam will see as if it were traversing through water. An example would be, if X amount of radiation penetrated 10 cm of water that would be its water equivalent depth. However, if that same amount of radiation were to be delivered to a denser material such as bone, that radiation may only penetrate 7 cm, similarly in lung tissue that is less dense than water it may transverse 11 cm. Then in the bone the radiological path length or water equivalent depth would be 7 cm and similarly in lung would be 11 cm. What this shows is that the radiological path length is directly proportional to the

density of the material across which the radiation must traverse. All modern radiation oncology centers commission and benchmark both their linear accelerators and their treatment planning systems in big water tanks, this is also the recommendation of the American Association of physicists in medicine and commissioning the systems.[39-41]

In Figure 2.8, the particles physical geometrical path is defined as D. However, the radiological path length of the Ray is defined as the sum of the products of the density times the amount of distance traveled within that density. In radiation oncology that physical path length D is defined in water. The subsequent radiological distance d maybe longer or shorter than D depending on the densities that the Ray must traverse through and how much energy it loses. This path length or depth is sometimes referred to as water equivalent path length or water equivalent depth[26,42]

$$d = d1 * \rho1 + d2 * \rho3 + d3 * \rho4 + d4 * \rho6 \quad (2.17)$$

The radiological path length in Figure 2.8 of d1-d4 will be increased or decreased by the algorithm depending on if the density that the Ray must traverse is more or less dense than the benchmark of the Ray traveling in water.

For this study the algorithm that was used is patented by Varian medical systems and is called Anisotropic Analytical Algorithm (AAA). This algorithm computes dose in the form of energy transport inside a medium. The dose kernels scale themselves by adjusting to different radiobiological path lengths.

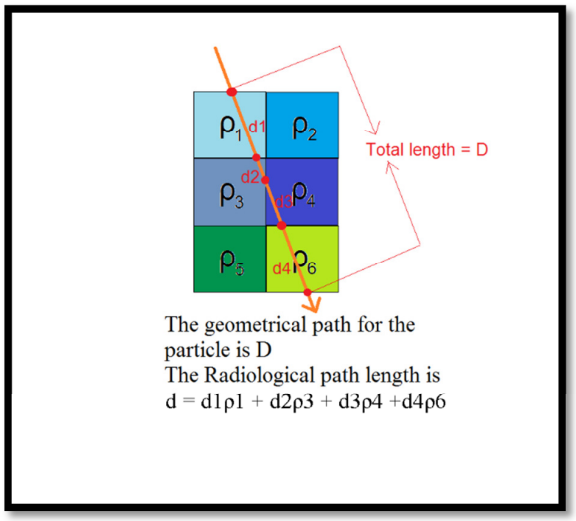

Figure 2.8 *Simple Ray tracing method displayed..*

Chapter 3

METHODS FOR 4D DATA ACQUISITION AND EXTRACTION

3.1 Volumatic change in lung data extraction.

This study would retrospectively analyze previously treated patients that had been simulated before treatment using 4DCT[32,43]. The full respiratory cycle of the patient would be then broken down into 10 breathing phases from 0% to 90%, where 0% and 90% would be the peak of inspiration and 40% would represent the patient fully inhaling. The radiation plan that was delivered to the patient would then be recomputed on the entire breathing phase and the dose volume histograms would be generated to evaluate the V5 and V20 dose end points. This would result in ten different treatment plans to evaluate for each patient.

The first step would be to determine if there's a correlation between the changes in the volume of the lung and the low dose region. This will determine the feasibility of this study and whether or not there is a requirement for it.

If the preceding step were to demonstrate that there is a significant change in the low dose region of the lung during treatment the next step would be to determine if it is, in fact, feasible to use CT numbers and Hounsfield units of a CT scan as a surrogate for the density of the tissue. The CT and Hounsfield units would then be examined to see if there is a reliable way in which the mass of the lung encapsulated by the dose volume can be interpreted through those numbers.

3.2- 4D dose calculation

The effort to compute a realistic representation of dose for patients receiving XRT (X-ray Radiotherapy) for target site that are in or near other dynamic organs continues to be a challenge in the community[44,45]. These challenges begin at the very beginning of treatment planning when Versteijne *et al.*[46] indicates that even the tumor site delineation is challenging. This transfers in treatment planning. The use of 4DCT and 4D treatment planning help reduce uncertainty during the treatment planning phase[47] and these improved calculation may lead to improved outcomes for patient with respect to treatment related toxicity[48].

Increasingly complicated treatment techniques have the potential benefits to reduce toxicity[49], their use has increased in the radiation oncology community. One of these is Intensity Modulated Radiotherapy (IMRT)[50]. Error rates in IMRT computed plan on dynamic organs is higher due to the dose accumulation effect of multiple gantry angles used for treatment and the beamlets used to optimize the radiation plan suffer from intrafraction dose uncertainty[51].

For Lung cancer a true cumulative dose would be a dose that can account for difference in dose distribution in all the breathing phases, however, most all modern radiation treatment planning systems (TPS) assume static patient geometry. This assumption of static anatomy and the dosimetric consequence is well known for many years[52]. However, a generalized and standardized method by which to account for these uncertainties has yet to be presented.

3.2.1 Algorithmic calculation 4D dose.

One of the ways that the has been proposed is that the process be archived algorithmically via deformation of the dose grid using Intensity-Based Free-form Deformation[53] to Monte Carlo simulations[54,55]. Without exploring the deformation process in too much depth, the processes involve a deformation grid[56] with certain coordinates (v_{ij}) and preforms a registration of field vectors with respect to their spatial relationship to each other. Then using the translation of the field vector registration and transformation the dose grids are transformed between CT geometries. This allows for the dose from one CT of a breathing phase to be transported and propagated through the remaining breathing phase CT and thus a more realistic representation of dose delivered to the patient.

3.2.2 Direct calculation and re-computation of 4D dose.

Direct calculation and re-computation of 4D dose is the method by which the treatment plan that is selected is copied on to each individual breathing phase and then recomputed in the TPS. This process allows for an evaluation of the dose distribution in clinically significant way and one that permits the user to visually examine the underlying anatomical deformation in real time. Also, this method is the most commonly applied technique when adaptive radiotherapy is used[57,58]. This is the method used to sample data in this research effort. For this study the reference scan that is used is the average intensity projection of all 10 breathing phases as explained in section 2.7. This allows for a static dose calculation on a total of eleven CT data set

and eleven different treatment plans per patient. Once these plans have been generated they are then mined for dosimetric and volumetric data.

3.3 Understand a Dose volume histogram

A brief overview and understanding of a Dose Volume histogram is required to understand why its use is so prevalent and wide spread in the radiation oncology community for both evaluating radiation dose prescription coverage and assessing risk of damage to uninvolved healthy tissue that the target may be close too[59].

3.3.1 Types of DVHs

The first important to note is that a DVH can only be generated for a 3D treatment plan, this includes a 4D treatment plan that is, as mentioned in previous sections, a series of 3D plans with a temporal component. To generate a DVH for 3DCT data set first requires the user to define and draw a contour on the CT data set. This contour or drawing is a visual representation of, either the target or other Organs at Risk (OARs). The dose value inside each of the voxels inside the defined contour are then sampled. A voxel is a three-dimensional pixel. As the volume of each voxel is known therefore the volume of the target of OAR is known. After the dose (in Gray (Gy)) is sampled, the data from for each of the voxels is the tabulated in a form of a standard histogram. This is done in either absolute dose or volume or in relative terms (%Dose or %Volume). Figure 3.1 is an example of two different treatment planning techniques being used on the same patient anatomy (it is worth noting that

these plans are test cases only and is used for demonstration purposes only). The plan in the left-hand side is using a conformal art technique, and the one on the left is using a traditional three field arrangement. On both plans the red contour is the target, the liver is contoured in Brown and the spinal cord in green. The goal of the treatment plan is to cover the maximum amount of the red contour with the yellow prescription isodose line (30 Gy). As is clear from the images the amount of coverage cannot be determined or compared visually. It is also difficult to assess how much each treatment technique is delivering to the organs at risk, in this case the liver and the spinal cord. This is where the DVH is a useful tool when quantitively assessing dose to OARs relative to target dose coverage.

As is clear in figure 3.1 that the plan on the right (with triangles on the DVH lines) has similar coverage of the target (red) as the one on the left (squares on DVH lines) but has a higher dose to the spinal cord (green). The clinician must now decide which of these plans will lead to a better patient outcome. As is also clear in the two plans DVHs overlapping, that the low dose region (5Gy) and the higher dose region (20Gy) are having opposite contributions to the liver. One plan delivers 5Gy to approximately 80% of the liver but only around 10% gets 20Gy and in the other plan 5Gy is received by approximately only 50% of the liver, however approximately 25% gets 20Gy. Difficult decisions like these are an everyday occurrence in radiation oncology clinic.

It is also worth noting in figure 3.1, the artifact of helical CT back projection accumulation that was discussed in section 2.5. It is because of this reason that if close attention is paid to the red contoured target volume it can be seen to extend into the lung despite there being no tissue density of the same value present. This is because this patient had also received a 4DCT to assess movement of the target

because it is so close to the diaphragm. The target was delineated using the respiratory cycle of the patient and therefore includes regions that would not be visible in this single snapshot of a 3DCT. Without the aid of a 4DCT there would be no way to delineate the target across the respiratory cycle. This would mean that when the target would move into the regions that are contoured inside the lung area they would not be effectively treated. This is another example that the advantages at 4DCT brings to treating dynamic organs.

This visual representation of dose relative to the volume of either the tumor or OAR can be displayed in either Cumulative DVH or a Differential DVH[60].

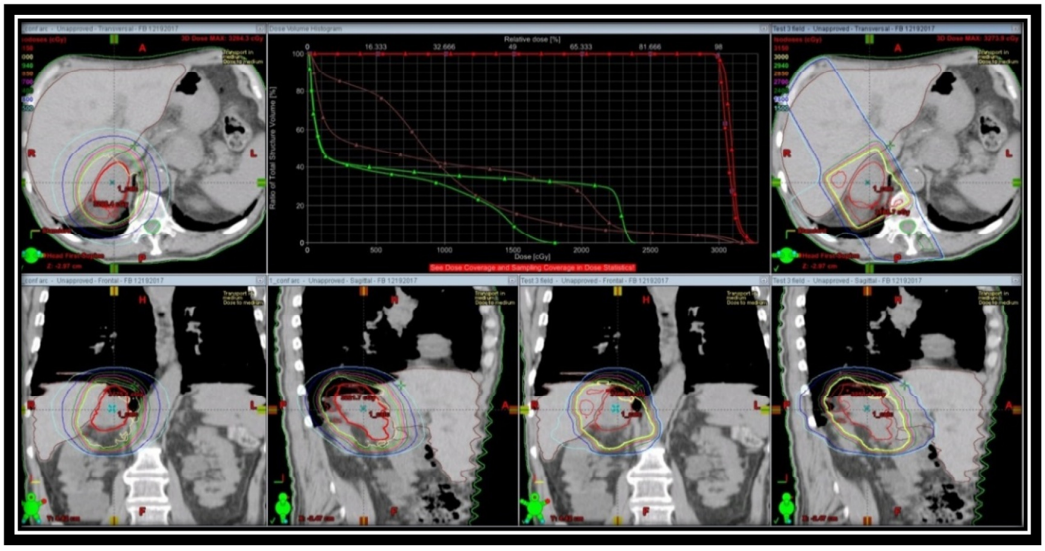

Figure 3.1 *Two different planning techniques on the same patient volume.*

The three images to the on the left of center displays a conformal arc technique and the three images on the right of center displays the uses the traditional three field technique. The central image is both plans DVHs is overlapped

3.3.1.1 Differential DVH

The differential DVH is like the generic form of a histogram that are prevalent in statistics. The difference form one differential DVH to the other is generally the width of the dose bins used. This is useful when evaluating a treatment plan because it is very easy to see the minimum and maximum doses. As the figure 3.2 shows the 0.5cm grid on the patient's anatomy with two contours (target in red and spinal cord in green), corresponds differential DVH of the dose received by the volumes drawn, displayed on the top right panel the figure. One of the advantage of the differential DVH is that the histogram it is useful when comparing different histogram with a varying bin size[60].

The disadvantage to the Differential DVH, however is that when comparing two contours of the same plan on the on same patient, it is difficult to extract meaningful clinical information. Figure 3.2 shows one of the treatment plans form the previous figure 3.1with the data extracted into a differential DVH in the top right corner displayed in red (target) and green (spinal cord) distributions. But is it possible to answer some simple question such as: How much of the spinal cord is receiving 15 Gy, or how much of the target is getting the prescribed 30Gy? These are important questions and the answers have critical clinical significance to patient outcome and toxicities. They can be answered as the data is embedded in the differential DVH however, it would require some more data manipulation. As the data is currently displayed, it is not possible to answer these questions easily.

The three images to the on the left of center displays a conformal arc technique and the three images on the right of center displays the uses the traditional three field technique. The central image is both plans DVHs is overlapped

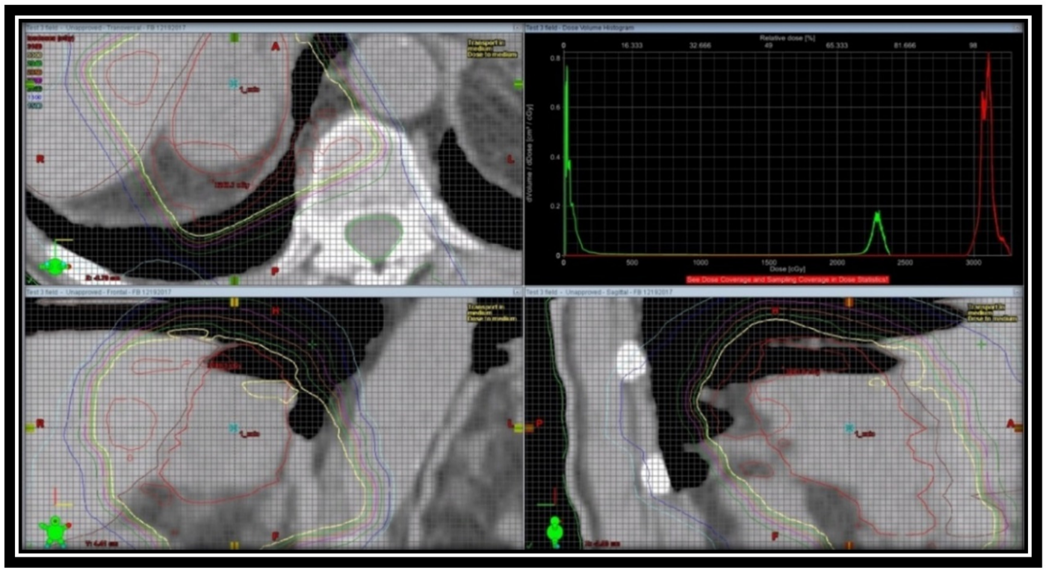

Figure 3.2 *Three field technique described in figure 3.1. Displayed on the axial sagittal and coronal images is a magnified view. In the top right corner is the differential DVH.*

3.3.1.2 Cumulative DVH

The cumulative DVH is the most commonly used histogram in all of radiation oncology. As with most histograms where we assume that there are k number of bins and n is the number of dose points sampled, then histogram h_i is given by:

$$n = \sum_{i=1}^{k} h_i \qquad (3.1)$$

The cumulative histogram of h_i would then be defined as H_i :

$$H_i = \sum_{j=1}^{k} h_j \qquad (3.2)$$

This process can be seen graphically in figure 3.3 below, where differential DVH is integrated until a cumulative DVH is achieved. In the figure the volume a

specific dose is plotted in a direct histogram. The cumulative DVH is created by integrating the histogram with the condition that it starts at 0% of the dose is being received by 100% of the volume and continues this to the maximum dose.

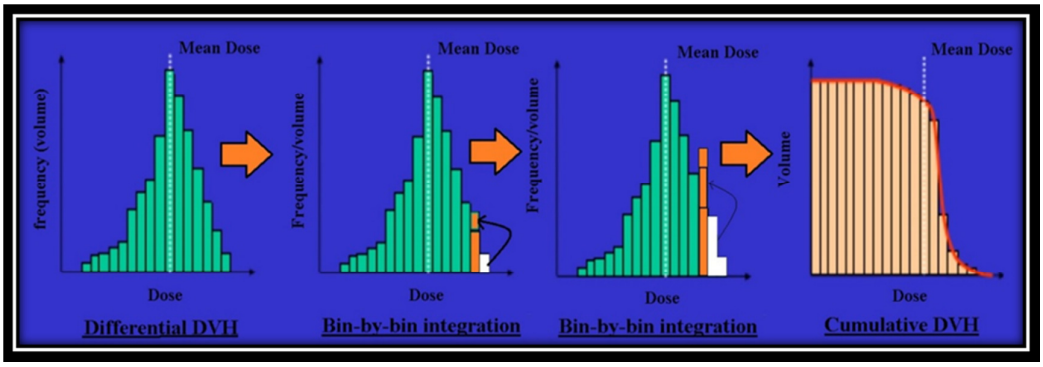

Figure 3.3 *This demonstrates the bin by bin integration of a differential DVH to arrive at a cumulative DVH.*

The advantage of this is that the scaling of the two volumes from the previous example can be observed in the upper right corner of figure 3.4. It now becomes easy to answer the questions previously proposed. How much of the spinal cord is getting 15 Gy? The answer is around 35% of the volume of the contoured spinal cord is receiving 15 Gy. And what is the percent of the target getting the prescription dose of 30 Gy? The answer is around 95% of the target is receiving 100 % of the prescription dose of 30 Gy.

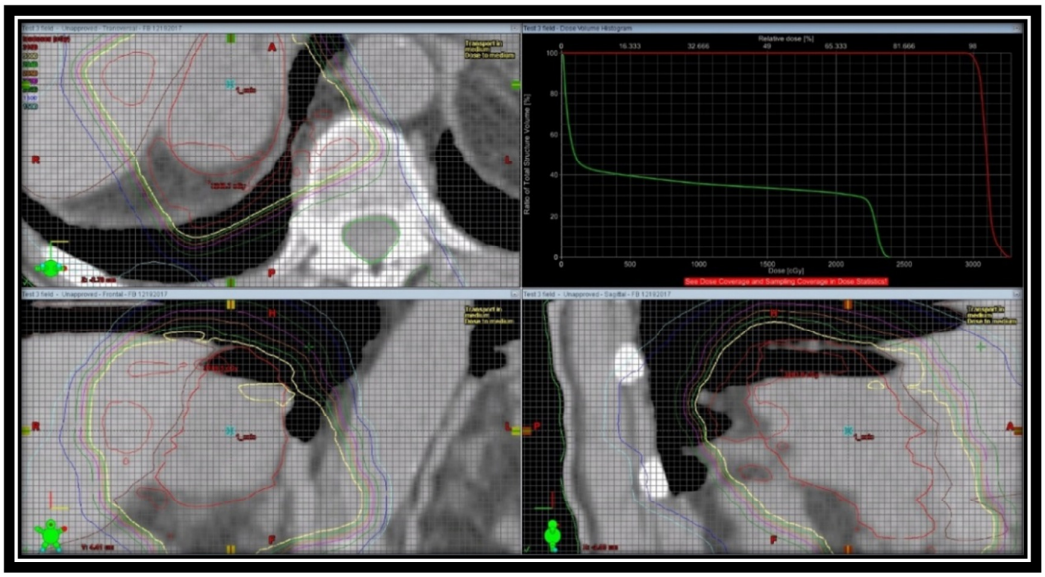

Figure 3.4 *As in figure 3.2 this is a magnified view of the same volume on the same 0.5 cm with in the top right corner is a cumulative DVH of the two volumes of interest.*

3.4 Interpretation of a DVH

3.4.1 Target dose coverage evaluation via DVH

Given the same example used in this section, the cumulative DVH can be used to assess both the OAR and target. In figure 3.5, the mean dose to the target exceeds the prescription of 30Gy. This is not an uncommon occurrence in radiation treatment plans. Target or tumors are routinely over treated so as to get the prescribed dose to the outer edges of the cancer[42,61]. These are referred to as "hotspots". The consequences are the tumors are "hotter" in the center than the periphery. These hotspots are allowed within reason and treatment planners are given guidance by the physicians and treatment protocol on how hot the hotspots are allowed to be. Similar guidance is given to what percentage of the tumor volume is allowed to get less than the prescription. The target is generally under-dosed to control the hotspot and/or

reduce the dose to the surround OARs that may be in danger of exceeding their allowed dose tolerance.

3.4.2 OAR dose sparing evaluation via DVH

Organ at risk or OAR sparing is one curtail objectives on any radiation treatment plan. The ultimate goal is to give the maximum amount of dose to the maximum amount to tumor and the least amount possible to the OARs. Unfortunately, that is not always possible. This is usually due to the proximity of the target to the organ at risk. In the case of this study, the targets are embedded in the organ that is the OAR. The OAR these cases of will the healthy lung tissue and since the tumors are embedded inside them, they are expected to receive significant dose to get the prescribed dose to the lung cancer.

These restrictions to dose have a specific nomenclature, specified by “V”s and “D”s followed by a number. For example, a V5, is defined as the percent of volume receiving 5 Gy. And similarly, D5 would the dose received by 5 % of the volume. As demonstrated in figure 3.5 the spinal cord has a V23 of 10% and similarly a D10 of 23Gy, as denoted by the orange line. The “D” are more generally used in brachytherapy, in X-ray radiotherapy it is more common to use the Vs as dose limiting tolerances for OARs. It is used to demonstrate the answers to the questions that are asked when evaluating a radiation treatment plan. The orange line represents the measure on the spinal cord of how much dose 10% of the volume is receiving. The straight yellow bar represents the mean dose to the target. The straight green line represents the prescribed dose to the target. The red DVH of the target beyond the

prescribed line is considered overdose and behind the green line is considered an under dose.

To this end there have been many efforts to try and understand what the "tolerance" of the OARs is to radiation. Meaning, how much dose can the healthy tissue absorb before losing some functionality, most functionality or all of its functionality. These biological end point have been explored from the first comprehensive guide by Emami *et al.* [61] and specially for lung is was Miles *et al.* [63] who talked about the need to restrict the high dose regions of the lungs but also showed a link to the lower dose regions and how they contributed to toxicity. This led to the multi institutional effect in the Quantitative Analysis of Normal Tissue Effects in the Clinic (QUANTEC)[64-68] which is now the gold standard in most all radiation oncology clinic can clinical trials.

Figure 3.5 *This is a maximized view of the cumulative DVH from figure 3.4.*

3.4.3 The pitfalls of relying too much DVH interpretation.

The first problem with evaluating a radiation treatment plan by just the DVH is that they are not likely to correctly represent a very high and potential problematic hotspot, this is also true with cold spots in the tumor. The cold spots could be a problem because it could be present in the middle of the tumor and because of the integral nature of cumulative DVH, it would be difficult to see where the cold spot could be. DVHs are also only as good as the volumes that are drawn by the user. If there was a mistake made by the user when identifying an organ or tumor volume, the DVH may show perfect tumor coverage and excellent OAR sparing but the reality would be different. There have been several studies that show that the difference of the same organ or tumor being contoured by multiple users can result in variation in the defined target[69,70]. One older study found that, although less pronounced as the inter-user variability, they have a measurable amount in intra-user variability[71]. Due to these potential problems and pitfalls it is important that it be recognized that the DVH is an important tool in the evaluation of radiation treatment plans, but it is only one of many that must be used to ensure that the plans are evaluated in the most thorough way possible.

3.5 Detail of data extraction from treatment planning.

3.5.1 – Patient selection

The first criterion for patient eligibility was related to disease sites. As the purpose of this study is to evaluate low and mid dose regions during radiotherapy in

and around the lung regions, only patients that had existing clinical radiation treatment plans in and around the lung region were deemed eligible and selective. The next criteria for selection was a function of how reliable or how accurate the 4DCT reconstruction was for the patient. As discussed in sections 2.6, 2.7 and 2.8 the very first step of a good temporally reconstructed three-dimensional volume begins with a continuous and reproducible breathing trace. The study used the Varian RPM system, which consists of an external marker placed on the patient's chest which is tracked by an infrared camera. The correlation between the movement of the chest and the acquisition of back projections in the CT scanner are crucial. Since the time period, the pitch, slice thickness and table feed speed are all set on the onset of data acquisition, if the patients breathing rhythm changes mid-scan or if the patient takes a deep breath, this can have dire consequences on the 4D image reconstruction. This consistency of the breathing pattern is presented to the user in the form of error bars per phase. Although this is a systematic error as discussed in sections 2.6, for the purposes of this study, since a reliable volume is crucial to data acquisition any patient with an error of more than 5% per phase was immediately excluded from the study. This was done to reduce the consequences of incorrect time periods resulting in image artifacts as demonstrated in figure 2.7. The results, as expected, were fewer artifacts due to breathing motion, and a more reliable data set upon which to base the volumes and doses.

3.5.2 Volume and Density extraction

Once the patient was selected and deemed eligible due to minimal potential reconstruction artifacts, the patient's 4DCT data set was reconstructed. This

reconstruction consisted of 10 breathing phases CT sets, starting at 0% breathing phase all the way to 90% breathing phase. Once the reconstruction was complete, the scans were examined to ensure minimal artifact, specifically, the reconstruction artifact that occurs near the diaphragm as discussed in section 2.5 and shown in figure 2.4 and figure 2.7. These 10 CT scans of the breathing phases were then used to create an average intensity projection scan. This average scan would be the one that would have been used for this patient clinically. Therefore, for the purpose of this study the scan would be the benchmark upon which the variation of volume and dose for the remaining 10 CT scans would be measured.

Only the lung contours were drawn using auto segmentation[72] to minimize contouring errors and to create a consistent workflow that could be reproduced among all patients. This was also done to minimize the potential for intra-user variability[71] in contouring volumes, as discussed in section 3.4.3. All of this data was then transferred to a MIMvista workstation for evaluation and data extraction. At the MIMvista station, using deformable registration and volume propagation. MIMvista was chosen as it has a very high performance in deformable image registration[73], the lung volumes from the average scan were propagated sequentially into the 10 breathing phases. Again, this was done to minimize error due to user interaction, and for the creation of the reproducible and consistent workflow for remaining patients. Once these volumes were created and labeled, volumetric and density extraction could begin.

The data output consisted of the integral Hounsfield units (HU*ml), maximum and mean Hounsfield units and the volume of the lungs. It is important to extract the volume for both lungs simultaneously, as most protocols and treatment clinical trials make recommendations for limiting lung dose to both lungs. Therefore, in the study

the volume analysis is taken for both lungs rather than just the disease affected lung. This data is extracted for the lung contours in all 10 phases and the average CT scan and tabulated. Table 3.1 below is an example of these data extracted points tabulated for a single patient. Tabulation is done with the CT data set listed in the first column proceeded by the data extracted from it.

CT set Pt#1	Integral Total (HU*ml)	Max (HU)	Mean (HU)	Volume (ml)
AvgCT	-3339088.25	677	-741.85	4501.05
PH00	-3729015.5	706	-763.3	4885.37
PH10	-3601915.5	816	-754.31	4775.13
PH20	-3435660.25	795	-747.66	4595.24
PH30	-3345598	803	-745.13	4489.94
PH40	-3272909.25	800	-740.4	4420.44
PH50	-3231061.75	807	-737.23	4382.71
PH60	-3193081.5	815	-735.06	4343.97
PH70	-3199652.5	840	-733.95	4359.47
PH80	-3373558	837	-741.43	4550.04
PH90	-3553407.25	818	-754.22	4711.34

Table 3.1 *Example of the tabulated data from the first of the 10 patients selected for the study*

In table 3.1, the integral Hounsfield units (HU*ml) is not needed for this study and the Max HU are also not relevant. The only data from the volumetric extraction that is used is the Mean HU and the Volume.

3.5.3 - DVH generation and dose volume extraction

Once the volumes have been generated and Hounsfield units and volumetric information extracted, all 11 CT scans were then exported to the Varian Eclipse

treatment planning system. Once there, the patient's clinically delivered radiation treatment plan was then transferred to the average CT data set and recomputed. The same radiation plan was also transferred to all 10 breathing phases and recomputed as well. Then from each of these treatment plans DVHs were regenerated for the lungs. Those DVH is were extracted in tabular form and the volumetric dose points the V5, V10 and V20 were exported into Microsoft Excel for further analysis.

Institution	Paper title	Points evaluated	Ref.
London Regional Cancer Program, Ontario Canada	Predicting Radiation Pneumonitis After Chemoradiation Therapy for Lung Cancer: An International Individual Patient Data Meta-analysis.	V5, V20	[74]
Washington University	Toxicity and outcome results of RTOG 9311: A phase I–II dose-escalation study using three-dimensional conformal radiotherapy in patients with inoperable non–small-cell lung carcinoma	V20	[75]
Duke University, North Carolina	Radiation-induced pulmonary toxicity: a dose-volume histogram analysis in 201 patients with lung cancer.	V10, V30	[8]
Peking University China	Analysis of clinical and dosimetric factors associated with severe acute radiation pneumonitis in patients with locally advanced non-small cell lung cancer treated with concurrent chemotherapy and intensity-modulated radiotherapy	V10	[76]
Aarhus University Hospital, Aarhus, Denmark.	New dose constraint reduces radiation-induced fatal pneumonitis in locally advanced non-small cell lung cancer patients treated with intensity-modulated radiotherapy.	V5, V20	[11]
MD Anderson Houston Tx	Analysis of clinical and dosimetric factors associated with treatment-related pneumonitis (TRP) in patients with non–small-cell lung cancer (NSCLC) treated with concurrent chemotherapy and three-dimensional conformal radiotherapy (3D-CRT)	V5	[77]
Multi-institutional	Quantitative Analyses of Normal Tissue Effects in the Clinic (QUANTEC): an introduction to the scientific issues	V5, V20	[78]
Fujian Medical University China	Dose-volumetric parameters for predicting severe radiation pneumonitis after three-dimensional conformal radiation therapy for lung cancer	V5, V10, V20, V30	[79]

Table 3.2 *Small samples of literature and outcome studies and the lung dose point examined or recommended.*

The V20 is the most commonly used data point to assess and evaluate the probability of healthy lung developing radiation-induced pneumonitis[80]. However, after a brief literature search on recommended tolerances for healthy lung tissue, some of which have been tabulated in table 3.2, it is clear that the V5 and V20 are commonly quoted tolerance points for lungs in treatment protocols and clinical trials. The V10 is also mentioned in some paper as an end point but not as often as the V20 and V5, so it was chosen as an intermediary point between the two commonly recommended values so as to assess if was any trend to the data.

Once the three dose points were extracted they were tabulated as can be seen in table 3.3. With the first column representing the phase of the CT scan starting with the average scan, followed by successive columns of the dose points

The steps and procedures were then repeated for the remaining nine patients, all the pertinent volumetric extraction and dosimetric extraction was done and tabulated. The analysis of this data and further discussion can be found in the next chapter

CT set	V5(%)	V10(%)	V20(%)
AvgCT	19.23	13.11	7.19
PH00	18.49	12.57	6.85
PH10	18.49	12.57	6.94
PH20	19.17	13.05	7.14
PH30	19.32	13.17	7.22
PH40	19.44	13.25	7.26
PH50	19.48	13.28	7.31
PH60	19.49	13.26	7.29
PH70	19.40	13.18	7.25
PH80	18.96	12.88	7.08
PH90	18.83	12.75	6.94

Table 3.3 *Tabulation of all dosimetric data points. All numbers are expressed in % of the total volume of the patient's lungs. The tabulated data represents the % of total lungs volume receiving 5Gy, 10Gy and 20Gy.*

.

3.5 Finite Element modeling

The concept of fine element modeling was also explored for its applicability in assisting in volumetric analysis for this study. The finite element method is a numerical based method applied to analysis of structural integrity fluid dynamics to name a few. Applications of this method have also been used in analysis in the biomechanics of respiratory lung motion as early as the 70s and 80s[81-85]. There are several other more recent example of the use these of the use methods and computer topography based analysis in modeling the bronchial tree[86] and others where simulations of the respiratory system were used to diagnose respiratory disease[87]. More recent examples can be found where Werner *et al.* used a patient specific methodology and four DCT imaging to model the lung motion and patience during respiration[88].

However, this image-based segmentation and detection approach, was not ultimately applied to the study. The primary reasons being that it could only be used to extract volumetric data from the lungs. It would not be helpful or useful in defining or extracting the V5, V10 and V20s that come from the treatment planning software. In order to extract dose information from radiation treatment planners using software other than provided by the vendor would also be problematic. Radiation treatment planners are considered FDA approved medical devices and any changes or alterations to their source code is prohibited.

So that would mean that one of the volume data sets would come from finite element analysis and the others would come from tradition contouring software. That may be in danger of raising some "consistency of measurements" against the data. And therefore, this technique was not explored further.

Chapter 4

DISCUSSION AND ANALYSIS

The motivation for selecting 10 patients is that this is a feasibility study to first, examine the extent of the shortcoming with the currently practiced ways of assess dose to healthy lung tissue and secondly, to compare it a more realistic approach of assessing dose to the mass lung versus dose to volume. The changing volumetric dose points is not in question, rather, this study will contrast each of the dose points within the patient and compare them to newly achieved points inside the very same patient for the very same CT scan set. The goal is that this, potentially reproducible metric, that can be used to evaluate the same recommended dose points but in a new way. For this hypothesis to be reliable it must prove true on every patient.

As will be discussed later in this chapter, ten patients will yield 110 CT scans and similarly, 110 radiation treatment plans. Each CT set and treatment plan will yield 4 volumetric data point and 4 Mass data points, which will lead to each patient generating 88 data points and a total of 880 points from all 10 patients. All the raw data collected can be found at the end of this document.

4.1 Acquiring Dosimetric data in Combining with Volumetric data

The previous section 3.5.2 discusses how to extract the density and volume information from each patient with an example of the first patient in table 3.1. The

next steps in data acquisition are to send all of the CT data sets and the all of the volumes to the Treatment planning system. Once imported into the treatment planning system, each patient's clinically administered radiation treatment plan is copied on the each of the 11 CT scan and recomputed. This work flow can be seen below in figure 4.1.

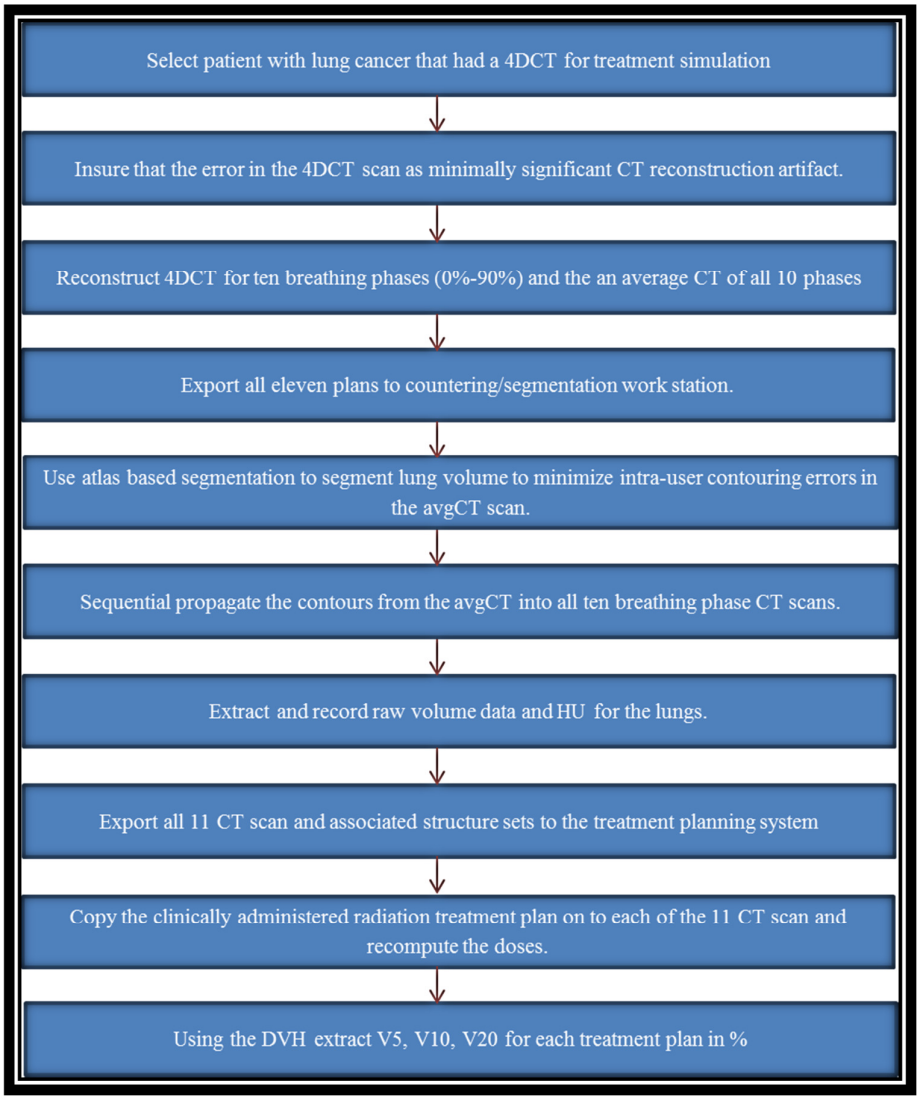

Figure 4. 1 *Workflow of volumetric data extraction from patients CT data*

This is followed by an analysis to generate and test reproducible trend that the relative change in volume of each patient has with the relative change in the three

dosimetric data points. This raw data can be seen below in table 4.1. It lists the mean Hounsfield units the volume of the total lungs, the percent of volume receiving 5 Gray, 10 Gray and 20 Gray respectively. The contextual content of the V5, V10 and the V20 are explained in section 3.4.2 and their relationship to the average CT and relative changer demonstrated in table 3.3.

Pt 1	Mean (HU)	Volume (ml)	V5 (%)	V10(%)	V20(%)
AVG	-741.85	4501.05	19.23	13.11	7.19
PH00	-763.30	4885.37	18.49	12.57	6.85
PH10	-754.31	4775.13	18.49	12.57	6.94
PH20	-747.66	4595.24	19.17	13.05	7.14
PH30	-745.13	4489.94	19.32	13.17	7.22
PH40	-740.40	4420.44	19.44	13.25	7.26
PH50	-737.23	4382.71	19.48	13.28	7.31
PH60	-735.06	4343.97	19.49	13.26	7.29
PH70	-733.95	4359.47	19.40	13.18	7.25
PH80	-741.43	4550.04	18.96	12.88	7.08
PH90	-754.22	4711.34	18.83	12.75	6.94

Table 4. 1 *Raw extracted data for first patient (Pt 1)*

To view the trend, the rate of change in lung volume of each 10 phase with respect to the average CT scan is tabulated for analysis in table 4.2. As is clear from the rate of change numbers there is a clear relationship between how, as the volume of the lung changes these previously perceives static dose points very across all 10 phases of breathing. Meaning that as the patient inhales the amount of dose being received increase, but just be the percent of volume. These trends were seen for all 10 patients, making them consistent variants inside the data point. This trend can be seen for patient one plotted in figure 4.2, where the rate of change of the lung volume is contrasted with the rate of change of the data points. As can be seen, the well-established fact that the volume of the lung can change up to 8% from the average in this patient also that the rate of change of the dose points can vary up to 4% as well.

These trends were observed across all 10 patients when their raw data subjected to similar calculations and tabulated to investigate similar trends.

Table 4.2 demonstrates the way in which these data from table 4.1 can be put into perspective, which is assessing all the data point as function of the relative change from the avgCT scan, as that is the benchmark planning CT that this patient would have their radiation treatment plan developed on and then delivered.

Pt1	% change in Lung Volume	% change in V5	% change in V10	% change in V20
PH00	-8.54%	3.82%	4.15%	4.61%
PH10	-6.09%	3.82%	4.15%	3.22%
PH20	-2.09%	0.31%	0.47%	0.67%
PH30	0.25%	-0.51%	-0.43%	1.09%
PH40	1.79%	-1.12%	-1.03%	0.23%
PH50	2.63%	-1.34%	-1.31%	-0.41%
PH60	3.49%	-1.34%	-1.13%	-0.17%
PH70	3.15%	-0.90%	-0.56%	-0.38%
PH80	-1.09%	1.39%	1.77%	0.54%
PH90	-4.67%	2.05%	2.72%	3.05%

Table 4. 2 *Relative change with respect to avgCT*

The advantage of observing the relative rate of change across the 10 selected patients rather than absolute change is that as will be discussed in the preceding sections 4.2, there is a large range for the total mass and volume of lungs in human adults. For this reason, a rate of change is a more reasonable approach when comparing different sizes of lung to each other. The other advantage is that when we compare the changes of the volumetric dose points to the mass dose points within the same patient, it a standard metric by which both can be compared.

As was shown in table 3.2 in Chapter 3, these dose points are used as limiting dose factors when recommending dose tolerances of the lung volume. The literature that is quoted in in table 3.2 does not allow for a variation within the breathing phases. Those protocols and papers, like all other dose recommendations for non-dynamic

part of the body; they treat these data points as static entities. As can easily be seen in patient 1 through 10 these data points are not static. As demonstrated for patient 1 in table 4.2 and figure 4.2.

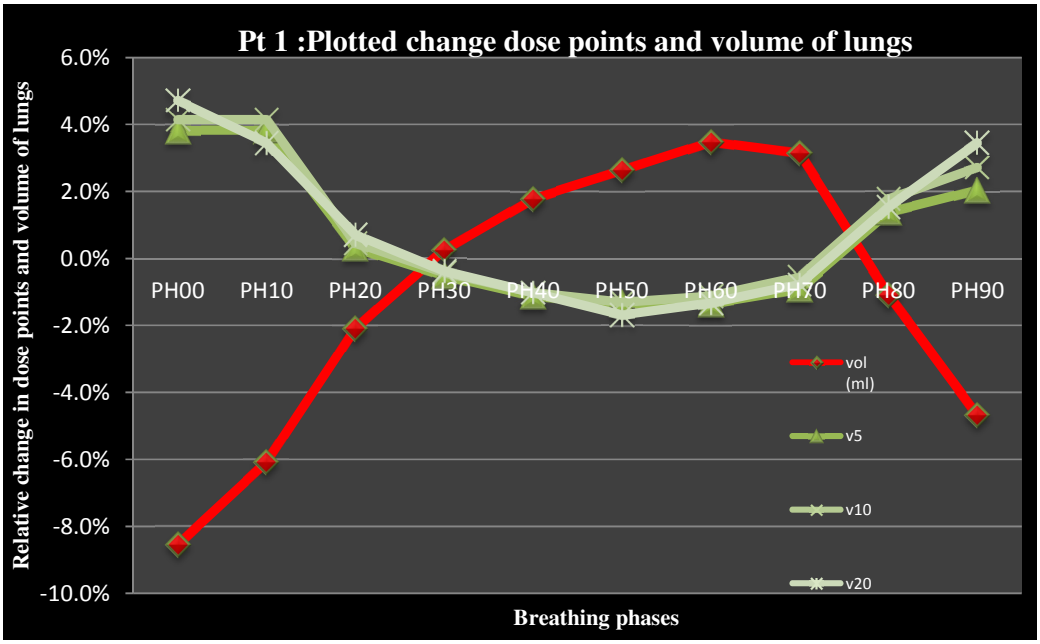

Figure 4. 2 *Relative change from table 4.2 plotted (Volume curve is inversed for contrast)*

The behavior of V5 through V20 is consistent with what was hypnotized. By definition radiation dose absorption is defined as Energy absorbed per unit mass. As shown in section 2.9.2 of Chapter 2, equation 2.16 shows the SI definition of radiation absorbed dose, Gray, as a function of Joules per kilogram

$$Gray\ (Gy) = \frac{J(joules)}{Kg(kilogram)} \qquad (2.16)$$

When a tumor volume is being treated in a particular part of a lung, with the radiation incidence from multiple angles the density of lung being exposed to the to radiation changes through the breathing various breathing phases. As explained in section 2.9.4, most treatment planning algorithms uses “mass stopping power” along the beam path to compute dose absorption. The mass stopping power is the physical

property of a medium of a specific density to absorb a specific amount incident radiation in a unit distance, per unit density. So, the rate at which the dose will be absorbed will be different. This difference in absorbed dose rate directly impacts the dose points V5-20 proportionally to the change in volume. This proportion will be different in each patient as the breathing tidal volume varies from one patient to the next. Tumor location is also affecting the change in the dose points. If the tumor location is very apical in the chest cavity, there is very little change in volume of the chest cavity at that location during inspiration. Chest is important as the "lung" contour is recommended to be drawn and identified as everything inside the chest wall region, not just visible lung volume.

4.2 Extraction of physical mass and density from raw data.

With the volumetric extraction complete, the next steps include efforts to extract the mass in grams of the lung volumes using the Hounsfield units. The relationship between the CT it intensity attenuation through a body and how those back projections are translated into Hounsfield units was demonstrated and discussed in section 2.3.

Similarly, using the information in table 4.1, that is the mean Hounsfield units for each phase of lung volume and the average CT scan, the density of the lung in grams/cm^3 is extracted using equation.

$$\text{HU} = \frac{\mu_{CT} - \mu_{CT\,(H2\,O)}}{\mu_{CT\,(H2\,O)}} * 1000 \qquad (2.12)$$

Although HU are a ratio of the linear attenuation coefficient, it was demonstrated in section 2.9.4 that this attenuation is a function of the density of the material that the radiation must traverse. Therefore, the assumption is made that the ratio of linear attenuation would equivalent to the ratio of densities. Then since equation 2.12 is dimensionless it can be rewritten as

$$\text{HU} = \frac{\rho CT - \rho CT\,(H2\,O)}{\rho CT\,(H2\,O)} * 1000 \tag{4.1}$$

And solving for ρCT leads to

$$\rho CT = \left(\frac{HU\,.\,\rho CT(H2\,O)}{1000}\right) + \rho CT(H2\,O) \tag{4.2}$$

The density water is 1 gm/cm^3

$$\rho CT = \left(\frac{HU\,.\,1}{1000}\right) + 1 \tag{4.3}$$

To this end the mean Hounsfield units extracted in table 4.1 are assumed to be an accurate representation of the entire lung volume. Once the density is extracted using equation 4.3, the volume information of each lung is used to extract the mass in grams using the simple equation of density.

$$\rho CT = \frac{Mass}{Volume} \tag{4.4}$$

This can be seen for patient one in table 4.3, along with both the standard and average deviations. It is worth noting that the standard and average deviations that are in recorded in table 4.3 do not include the average CT, rather only the 10 breathing phases labeled PH00 through PH10.

Pt1	Mean (HU)	Volume (ml)	Mass of Lung (gm)
AVG	-741.85	4501.05	1161.95
PH00	-763.30	4885.37	1156.37
PH10	-754.31	4775.13	1173.20
PH20	-747.66	4595.24	1159.56
PH30	-745.13	4489.94	1144.35
PH40	-740.40	4420.44	1147.55
PH50	-737.23	4382.71	1151.64
PH60	-735.06	4343.97	1150.89
PH70	-733.95	4359.47	1159.84
PH80	-741.43	4550.04	1176.50
PH90	-754.22	4711.34	1157.95
SD DEV	**9.10**	**178.42**	**9.84**
AVG DEV	**7.68**	**152.32**	**7.63**

Table 4.3 *Table HU, volume and extracted mass of lung computed along with Standard and average deviation*

The results of the masses for all the lungs in all 10 patients is consistent with published data on the weight of human lung in grams[31]. The referred published literature states that lung mass in adults can range from 371gram to 1852gram for both lungs together, with the average mass being 840 grams. For the 10 patients' average mass for all 11 scans ranged from 440 grams to 1162 grams with a mean of 645.40 grams.

4.3 Rate of change of total mass and volume of the lung.

The rate of change of the volume of the lung within each phase has already been recorded but to analyze the rate of change of the mass versus the volume, it is more perceptive to normalize the 10 breathing phases to the initial phase PH 00. This is done to demonstrate an initial zero y-intercept were the zero phase normalizes to itself and how the relative changes occur from that point forward. This is tabulated below in table 4.4 and graphically represented in figure 4.2. As the figure shows the

relative change in the mass is less prominent than that of the volume, this is as expected and hypothesized.

Pt1	Volume (ml)	Mass(mg)
PH00	0.00%	0.00%
PH10	-1.46%	2.26%
PH20	-0.28%	5.94%
PH30	1.04%	8.09%
PH40	0.76%	9.52%
PH50	0.41%	10.29%
PH60	0.47%	11.08%
PH70	-0.30%	10.76%
PH80	-1.74%	6.86%
PH90	-0.14%	3.56%

Table 4.4 *percent relative change in volume and mass with respect to PH00 phase*

The trend line for the rate of change of mass in the data plotted below in figure 4.3 reveals the line equation of y = -0.0003x + 0.0006, where the slope of -0.0003 indicates a fairly flat line. This is a trend that is observed across all 10 patients, with the highest variation of slope being -0.0032 in patient number five and the smallest being -0.0006 in patient number 10. Table 4.5 shows the line equation for all the change in total lung mass relative to the first breathing phase (PH00) for all 10 patients.

Patient number	Line equation for Change in Mass
Pt1	y = 0.0003x - 0.0006
Pt2	y = 0.0013x + 0.0131
Pt3	y = -0.0028x + 0.024
Pt4	y = -0.0012x - 0.0005
Pt5	y = -0.0032x + 0.0085
Pt6	y = -0.0005x + 0.0051
Pt7	y = -0.0029x + 0.0077
Pt8	y = -0.0004x + 0.0131
Pt9	y = -0.002x + 0.0133
Pt10	y = -0.0006x + 0.0069

Table 4.5 *All patients Line equation for Change in mass for all 10 patients with the relative change with respect to the first breathing phase (PH00).*

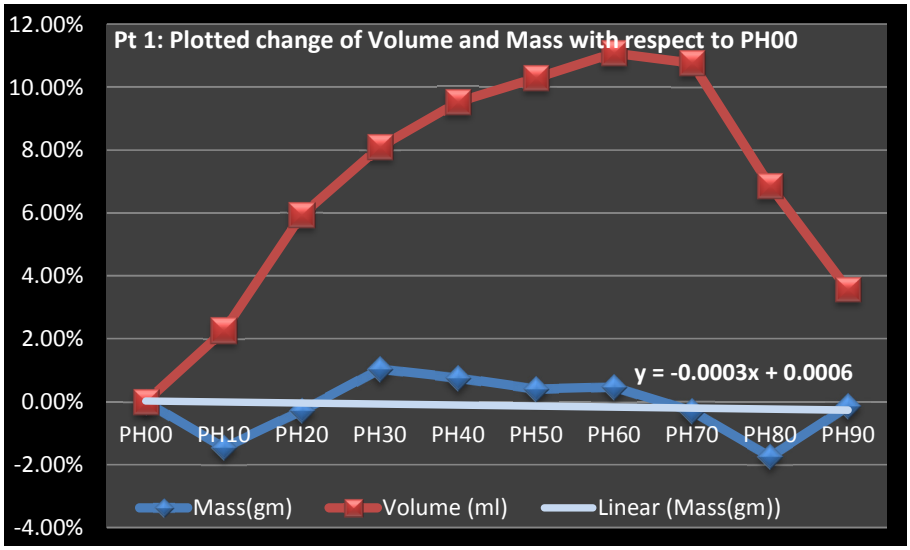

Figure 4. 3 *Plot of Table percent relative change in volume and mass with respect to PH00 phase.*

If the relative change of the mass and volume are then compared to the benchmark average CT scan upon which most treatment planning techniques are based, the hypothesized trend begins to emerge. Table 4.6 below lists the standard deviation of the mass of each patient with the volume of each patient. To evaluate and ensure the last of a systematic error in get acquisition it is worth exploring the rate of change of the volume and mass with respect to the zero phases as was done in table 4.4 but also the rate of sequential change from one phase to the next. One sees rate of change data were tabulated the standard deviation for both variation and mass and variation in volume were collected. The preceding two tables 4.7 and 4.8 are those observations of relative change and tabulates standard deviations when the 10 phases are compared to the peak breathing phase of PH40, and table 4.8 compares the sequential change from one breathing phase to the next. All three different techniques

reveal that the standard deviation of the rate of change of mass in the lung is less than 2% versus the volume.

Std Dev of % change relative to AVG	Mass(gm)	Std Dev of % change relative to AVG	Volume (ml)
Std Dev PT1	0.89%	**Std Dev PT1**	4.18%
Std Dev PT2	0.91%	**Std Dev PT2**	4.38%
Std Dev PT3	1.35%	**Std Dev PT3**	4.47%
Std Dev PT4	0.91%	**Std Dev PT4**	6.15%
Std Dev PT5	1.04%	**Std Dev PT5**	4.35%
Std Dev PT6	0.32%	**Std Dev PT6**	3.97%
Std Dev PT7	1.11%	**Std Dev PT7**	3.07%
Std Dev PT8	0.69%	**Std Dev PT8**	2.80%
Std Dev PT9	1.69%	**Std Dev PT9**	5.16%
Std Dev PT10	0.48%	**Std Dev PT10**	4.65%

Table 4.6 *standard deviations of the rate of change of the mass in the volume for all 10 patients relative to the average CT scan*

Std Dev of %change relative to PH 40	Mass(gm)	Std Dev of %change relative to PH 40	Volume (ml)
Std Dev PT1	0.90%	**Std Dev PT1**	4.25%
Std Dev PT2	0.87%	**Std Dev PT2**	4.41%
Std Dev PT3	1.37%	**Std Dev PT3**	4.65%
Std Dev PT4	0.92%	**Std Dev PT4**	6.39%
Std Dev PT5	1.13%	**Std Dev PT5**	4.61%
Std Dev PT6	0.32%	**Std Dev PT6**	4.07%
Std Dev PT7	1.12%	**Std Dev PT7**	3.12%
Std Dev PT8	0.68%	**Std Dev PT8**	2.86%
Std Dev PT9	1.72%	**Std Dev PT9**	5.26%
Std Dev PT10	0.48%	**Std Dev PT10**	4.80%

Table 4.7 *Standard deviations of the rate of change of the mass in the volume for all 10 patients relative to the Peak breathing phase CT scan*

Std Dev of sequential % change	Mass(gm)	Std Dev of sequential % change	Volume (ml)
Std Dev PT1	1.08%	**Std Dev PT1**	2.56%
Std Dev PT2	0.78%	**Std Dev PT2**	2.61%
Std Dev PT3	1.30%	**Std Dev PT3**	2.51%
Std Dev PT4	1.17%	**Std Dev PT4**	3.70%

Std Dev PT5	0.47%	**Std Dev PT5**	2.56%
Std Dev PT6	0.42%	**Std Dev PT6**	2.35%
Std Dev PT7	1.09%	**Std Dev PT7**	1.66%
Std Dev PT8	0.62%	**Std Dev PT8**	1.55%
Std Dev PT9	1.83%	**Std Dev PT9**	3.10%
Std Dev PT10	0.71%	**Std Dev PT10**	2.81%

Table 4.8 *Standard deviations of the rate of change of the mass in the volume for all 10 patients relative to the sequential normalization from one phase to the next.*

4.4 Extraction of volumetric and mass quantities from dosimetric points.

As demonstrated by the literature in table 3.2, the interest in the volumetric dose points clinically is defined in the percent of volume relative to the entire lung. For the purpose of this study, it is also important to look at the absolute volume of lung receiving the three dose levels of 5,10 and 20 Gray. This is done simply by extracting from the total lung volume the percent described for each point in the raw data. This is tabulated below in table 4.9.

Pt 1	V5 in absolute cm^3	V10 in absolute cm^3	V20 in absolute cm^3
avgCT	865.43	590.13	323.69
PH00	903.40	613.96	334.80
PH10	883.02	600.10	331.54
PH20	880.76	599.66	328.11
PH30	867.66	591.19	324.12
PH40	859.42	585.50	321.14
PH50	853.93	582.16	320.51
PH60	846.42	575.98	316.52
PH70	845.75	574.76	315.93
PH80	862.69	586.00	322.20
PH90	887.33	600.92	327.14

Table 4.9 *Absolute Volume of dose points receiving the three dose levels of 5,10 and 20 Gray extracted by the use of mean HU of individual CT phases and*

Pt 1	M5(gm)	M10(gm)	M10(gm)
avgCT	223.41	152.34	83.56
PH00	213.84	145.32	79.25

PH10	216.95	147.44	81.46
PH20	222.25	151.32	82.80
PH30	221.14	150.68	82.61
PH40	223.11	152.00	83.37
PH50	224.39	152.97	84.22
PH60	224.25	152.60	83.86
PH70	225.01	152.91	84.05
PH80	223.07	151.52	83.31
PH90	218.09	147.69	80.41

Table 4.10 *Tabulation of the mass of M5 M10 and M20*

Then using the mean Hounsfield of each CT scan tabulated in table 4.1 and the techniques described in section 4.2 of this chapter, it is now possible to estimate the mass of the lung volume receiving 5, 10 and 20 Gray. These masses, expressed in grams, can be seen in table 4.10. The new terms M5, M10, and M20 are designating the mass, in grams, of the lung receiving 5, 10 and 20 Gray, respectively.

4.5 Data Analysis interoperated data points.

4.5.1 Standard and average deviation of Lung mass and volume.

With the masses of these dose points are extracted their rate of change through the phases relative to the average CT scan are calculated below in table 4.11 and tabulated with the rate of change of mass and volume as a reference.

Pt1	*Volume (ml)*	Mass(gm)	m5	m10	m20
PH00	*-8.54%*	0.48%	4.29%	4.61%	5.16%
PH10	*-6.09%*	-0.97%	2.89%	3.22%	2.52%
PH20	*-2.09%*	0.21%	0.52%	0.67%	0.91%
PH30	*0.25%*	1.51%	1.02%	1.09%	1.14%
PH40	*1.79%*	1.24%	0.14%	0.23%	0.23%
PH50	*2.63%*	0.89%	-0.44%	-0.41%	-0.79%
PH60	*3.49%*	0.95%	-0.38%	-0.17%	-0.36%
PH70	*3.15%*	0.18%	-0.72%	-0.38%	-0.59%
PH80	*-1.09%*	-1.25%	0.15%	0.54%	0.30%
PH90	*-4.67%*	0.34%	2.38%	3.05%	3.78%
STD DEV	***4.18%***	**0.89%**	**1.66%**	**1.76%**	**1.99%**
AVG DEV	***3.38%***	**0.66%**	**1.33%**	**1.43%**	**1.55%**

Table 4.11 *Rate of change for patient 1's mass dose points, along with the rate of change in mass of the total lung and total volume*

If the methods and techniques described above are applied to all 10 patients and the standard deviations extracted for all the patient's M values and V values and an average taken of the variation ± standard deviation is seen that the variation of V5 vs. M5 is 2.64 ± 1.03% vs 1.99 ± 0.48%, respectively. The average variation of V10 vs. M10 is 2.61 ± 0.94% vs 1.75 ± 0.49%, respectively. The average variation of V20 vs. M20 is 2.81 ± 1.38% vs 2.16 ± 0.67%, respectively.

4.5.2 Analysis of Two-Sample t-Test Assuming both Equal and Unequal Variances

The next step of the analysis is to be sure that there is a statistically significant difference between the rates of change in mass points versus the volume points. Rather than measure that for individual patients that would result in a sample size comparison of 10 points in each category to be compared to 10 point of the reciprocal category, all the data points for all patient in each category were compared to their corresponding data point. This is possible because the data that is being compared is a "rate of change" from the avgCT of the phases with the hypostasis that that the observed rate of change in the mass data points is less than the large changes seen on the volume points. For example, in comparing the rate of change in the total observed mass is independent of the physical mass of the lungs; we are only interested in how much it varies from the baseline avgCT. Similarly, the same is true for the rate of change in total lung volume. It is also important to note that the mass data points are extrapolated from the volume points that they are being compared too. Therefore, the this t-test also shows that the statistically significant difference between the two

corresponding data sets also shows that there was no systematic error in the process for data derivation when generating the data points.

t-Test: Two-Sample Assuming Equal Variances	*%Δ Mass vs % Δ Vol*	*% Δ M5 vs % Δ V5*	*% Δ M10 vs % Δ V10*	*% Δ M20 vs. % Δ V20*
Total Observations(100 each)	200	200	200	200
Hypothesized Mean Difference	0	0	0	0
df	198	198	198	198
t Stat	2.475	3.154	3.135	2.781
P(T<=t) one-tail	0.007	0.001	0.001	0.003
t Critical one-tail	1.653	1.653	1.653	1.653
P(T<=t) two-tail	0.014	0.002	0.002	0.006
t Critical two-tail	1.972	1.972	1.972	1.972

Table 4.12 *t-Test: Two-Sample Assuming Equal Variances comparing the measured change in Mass to the volume in the lung over the breathing phases and the complementary mass and volumetric dose points.*

So to this end two sets of t-tests were performed on this data. The t-test first assuming equal variance is shown in table 4.13 and then the second test assuming unequal variance for the comparative quantities shown in table 4.14. Both of the tests display a P value of less than 0.05.

t-Test: Two-Sample Assuming Unequal Variances	*%Δ Mass vs % Δ Vol*	*% Δ M5 vs % Δ V5*	*% Δ M10 vs % Δ V10*	*% Δ M20% vs. %Δ V20*
Total Observations(100 each)	200	200	200	200
Hypothesized Mean Difference	0	0	0	0
df	172	198	197	198
t Stat	2.475	3.154	3.135	2.781
P(T<=t) one-tail	0.007	0.001	0.001	0.003
t Critical one-tail	1.654	1.653	1.653	1.653
P(T<=t) two-tail	0.014	0.002	0.002	0.006
t Critical two-tail	1.974	1.972	1.972	1.972

Table 4.13 *t-Test: Two-Sample Assuming Unequal Variances comparing the measured change in Mass to the volume in the lung over the breathing phases and the complementary mass and volumetric dose points.*

As the results of the two t-tests show there is a statistically significant difference between the two complementary data points. Besides small variations in the t- statistic, the p-values are identical and all below 0.05. What this allows for is the assumption that the rate of change in mass and lung are varying at two different and statistically significant ways.

4.5.3 Analysis of variance (ANOVA)

It is also important to emphasize that since the mass data was extracted using the volumetric information as well that there isn't a correlation between the various numbers. Tables 4.12 below demonstrate that using an ANOVA single factor test that all the P values are below 0.05. This test is done comparing the rate of change of the volume and the mass of all 10 patients in all 10 phases, equating to 100 points for the expression of variation in volume and similarly hundred points that express the change in mass.

SUMMARY Anova: Single Factor	*%Δ Mass vs % Δ Vol*	*% Δ M5 vs % Δ V5*	*% Δ M10 vs % Δ V10*	*% Δ M20% Δ V20*
Total Observations(100 each)	200	200	200	200
Between Groups SS	0.008	0.008	0.008	0.008
Between Groups df	1	1	1	1
Between Groups MS	0.008	0.008	0.008	0.008
Between Groups F	6.126	9.947	9.830	7.733
Between Groups P-value	0.014	0.002	0.002	0.006
Between Groups F crit	3.889	3.889	3.889	3.889
Within Groups SS	0.273	0.154	0.154	0.195

Within Groups df	198	198	198	198
Within Groups MS	0.001	0.001	0.001	0.001

Table 4.15 *Anova single factor results of change in volume vs. the mass lungs relative to avg CT for totals and dose points.*

4.5.3 One sample t-Test

With this information in mind we have to try and analyze the rate of change of total mass, M5, M10 and M20. The goal would be to try and determine if the rate for variation of those points from the expect deviation from the mass of avgCT is purely by coincidence or if there is a statically measurable way in which the change could be analyzed. More importantly, we would like to see how much of a change there is from the hypothesized variation of 0%. Since all the rate of change points, be it %Δ of mass of the total lung or the M5 etc. each is referenced to its own avgCT measurement and we are looking at how all of the %Δ mass points vary from 0% it would allow for all of the 100 points of each data point (%Δ total mass, %Δ M5, %Δ M10 and %Δ M20) from all patients to be analyzed simultaneously. This step of the analysis can be performed by running a one sample t-test on the mass data point as can be seen in table 4.15.

Description	Mass	M5	M10	M20
Average value of data before change	0.794%	1.171%	1.352%	1.655%
Expected change from Average CT	0.000%	0.000%	0.000%	0.000%
Standard deviation of data since change	2.908%	2.800%	2.870%	3.196%
Number of data points since change	100.00	100.00	100.00	100.00
Student's T-Value	2.732	4.181	4.710	5.180
Probability that the change observed from 0% expectation seeing is only due to chance (two tail)	0.007463	0.000063	0.000008	0.000001

Table 4.14 *One sample t-Test of the rate of change in Total lung mass, M5, M10 and M20 relative to the average CT scan. The*

The one sample t-test is appropriate because, although it is a known fact that the actual lung mass does not change for any patient during a CT scan, this is to test whether or not the perceived relative change in the all the mass data points were significantly different from bench mark of the avgCT data set. What this data shows is the when a one sample t-test is performed on the percent change in total lung mass, all the p-values for two tail analysis are below 0.05 and this test statically shows that the assumption that there should be a close to 0% variation from the mean CT is valid.

Those distributions can be seen in plotted in figure 4.4. Each of the distribution appears to have a Gaussian distribution around an average mean of around 1.24%. As the hypostasized variation of the masses from the avgCT was 0%, there for the mean variation of all the rate of change mass point should also be 0%. The 1.24% variation from the expected 0% is more than likely due to uncertainties that were unavoidable given the current level of technology made commercially available to radiation oncology clinic that were used in the acquisition of data for this study. The biggest contributor to the variation is the use of the mean HU of the lungs to attribute mass the entire lung volume, and all the dose points. This is because the assumption treats the entire lung as a uniform density organ, which it is not. This assumption also has the potential to effect the collection of mass dose points. The source for potential error would be the aforementioned use of the overall mean HU. This is when the techniques and methods described in in section 4.2 of this chapter were used on the volumetric dose points to extract the mass information.

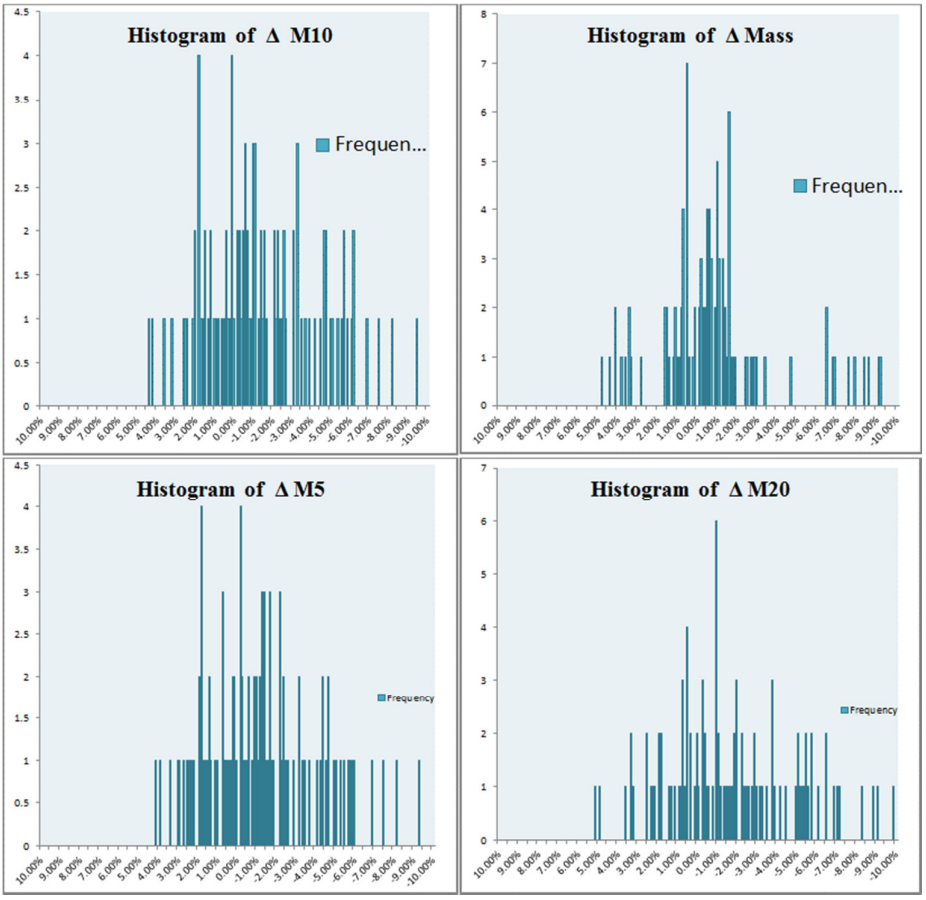

Figure 4. 4 *Separated histograms for plotting the change in total lung mass, the M5, M10 and M20 for all patients through all 10 breathing phases*

And just as a reference to evaluate the process, table 4.16 below is a one sample t-test of the rate of change for the total lung volume and volumetric dose points.

Description	Volume	V5	V10	V20
Average value of data before change	-0.505%	-0.072%	0.115%	0.422%
Expected change from Average CT	0.000%	0.000%	0.000%	0.000%
Standard deviation of data since change	2.908%	2.771%	2.704%	3.074%
Number of data points since change	100.00	100.00	100.00	100.00
Student's T-Value	1.736	0.259	0.426	1.374
Probability that the change observed from 0% expectation seeing is only due to chance (two tail)	0.085641	0.796338	0.670743	0.172627

Table 4.15 *For reference and to evaluate the process this table is a one sample t-test of the rate of change for the total lung volume and volumetric dose points.*

As is shown the p-values, using the two tail evaluation, show all the p-values are over 0.05. This is, of course, not a meaningful test because of the assumption that there would be no change or 0 % change of volume from reference avgCT, as it does in the mass change. The volume of a lung will, however change through a course of a single treat and, as this research effort shows, so do the volumetric data points.

4.5.4 Chi-square for variance

The next step would be to conduct a chi-square (χ^2) test to determine if the are some conclusions that can be reached about the variance in the data. The equation for the chi-square test for variance is given below.

$$\chi^2 = \frac{(n-1)S^2}{\sigma^2} \qquad (4.5)$$

Where,

n = sample size

S^2 = sample variance

σ^2 = Hypothesized population variance.

The one requirement for validity of this equation would be that it assumes that the data is normally distributed. The M5, M10 and M20 data histograms can be seen in figure 4.4 but a "goodness of fit" test must be conducted to determine if the data is normally distributed as this test is very sensitive to the normality of the distribution. That is to say, in data that are not normally distributed and have a small sample size the accuracy of this test can be questionable.

We assume the null hypothesis that the data is normally distributed, with the alternative that it is not. We then conduct the goodness of fit test. The result is P-value > 0.05 would mean that we do not reject the null hypothesis and the data is normally distributed. This was found to be true in the data, that is, the data for all 3 metrics, M5, M10 and M20 were normally distributed.

The test is demonstrated in table 4.16 for 100 data points for M5. We must first find the range via the minimum and maximum value. Then the cell length is found and rounded to 8 cell and then the data is sorted in cells and the chi-square values are computed by comparing the expected and observed frequencies. This was then repeated for M10 and M20 that can be seen in table 4.17 and 4.18 respectively.

M5	**Sample size 100.00**					
Min	-0.04					
Max	0.09					
Range	0.13					
cell length	0.02	Range/(1+3.22*log(sample size)				
Number of cell	7.64	(Range / cell length)		8(used number of cells		
corrected cell length	0.02					
Mean	0.01					
STD DEV S	0.03					
	Cell start	Cell end	Probability	Expected frequency	Observed frequency	CHI SQ
1st Cell	-0.04	-0.02	0.07	6.73	7.00	0.01
2nd Cell	-0.02	-0.01	0.14	14.36	17.00	0.49
3rd Cell	-0.01	0.01	0.22	21.66	24.00	0.25
4th Cell	0.01	0.03	0.23	23.09	26.00	0.37
5th Cell	0.03	0.04	0.17	17.41	8.00	5.09
6th Cell	0.04	0.06	0.09	9.28	12.00	0.80
7th Cell	0.06	0.08	0.03	3.50	4.00	0.07
8th Cell	0.08	0.09	0.01	0.93	2.00	1.23
Total					100.00	8.30
					Degrees of freedom(#cell-1)	7
					P-Value	**0.31**

Table 4.166 *Goodness of fit determination for M5.*

M10	Sample size 100.00					
Min	-0.04					
Max	0.09					
Range	0.14					
cell length	0.02	Range/(1+3.22*log(sample size)				
Number of cell	7.64	(Range / cell length)		8(used number of cells		
corrected cell length	0.02					
Mean	0.01					
STD DEV S	0.03					
	Cell start	Cell end	Probability	Expected frequency	Observed frequency	CHI SQ
1st Cell	-0.04	-0.03	0.06	5.71	4.00	0.51
2nd Cell	-0.03	-0.01	0.13	13.13	18.00	1.81
3rd Cell	-0.01	0.01	0.21	21.11	26.00	1.13
4th Cell	0.01	0.03	0.24	23.73	22.00	0.13
5th Cell	0.03	0.04	0.19	18.66	11.00	3.14
6th Cell	0.04	0.06	0.10	10.26	12.00	0.29
7th Cell	0.06	0.08	0.04	3.95	5.00	0.28
8th Cell	0.08	0.09	0.01	1.06	2.00	0.83
Total					100.00	8.13
					Degrees of freedom(#cell-1)	7
					P-Value	**0.32**

Table 4.176 *Goodness of fit determination for M10.*

M20	Sample size 100.00					
Min	-0.05					
Max	0.10					
Range	0.15					
cell length	0.02	Range/(1+3.22*log(sample size)				
Number of cell	7.64	(Range / cell length)		8(used number of cells		
corrected cell length	0.02					
Mean	0.02					
STD DEV S	0.03					
	Cell start	Cell end	Probability	Expected frequency	Observed frequency	CHI SQ
1st Cell	-0.05	-0.03	0.05	4.53	5.00	0.05
2nd Cell	-0.03	-0.01	0.11	10.91	11.00	0.00
3rd Cell	-0.01	0.01	0.19	18.76	24.00	1.46
4th Cell	0.01	0.02	0.23	23.07	24.00	0.04

5th Cell	0.02	0.04	0.20	20.27	14.00	1.94
6th Cell	0.04	0.06	0.13	12.73	13.00	0.01
7th Cell	0.06	0.08	0.06	5.72	5.00	0.09
8th Cell	0.08	0.10	0.02	1.83	4.00	2.56
Total					100.00	6.14
					Degrees of freedom(#cell-1)	0.52
					P-Value	**0.52**

Table 4.186 *Goodness of fit determination for M20.*

As is demonstrated by the results all p-values are greater than 0.05 showing that the data in all three sets is normally distributed. This is known as the Anderson-Darling Test in which because the p-value is greater than the significance level of 0.05, the decision is to fail to reject the null hypothesis. Therefore it cannot be concluded that this data does not follow a normal distribution.

With the establishment of the data being normally distributed the next step of conducting a chi-square test for variance can be done using the previously stated equation 4.5.

The data and calculations are tabulated in table 4.17 where the variance is first computed by a square root of the standard deviation of the 100 data point for each of the three metrics. The null hypothesis is that the rate of change data varies by less than 0.01% for each. Then to chi-square statics are computed by squaring the standard deviation, dividing it by the hypostasized variance and then multiplying the product by the degrees of freedom.

In the two tail test, if the p-value is less than half of the level of significance (0.05) then the null hypothesis is rejected. In this case, the null hypothesis is that the standard deviation of the rate of change in each of the data sets is 0.01%.

As can be seen in table the p-value of greater than 0.05 it can be concluded that there is insufficient evidence in the data that the standard deviation is of each of the data points is different from 0.01%.

DATA	M5	M10	M20
Variance	0.0008	0.0008	0.0010
Null hypothesis	0.0010	0.0010	0.0010
level of significance	0.0500	0.0500	0.0500
sample size	100	100	100
Standard dev.	0.0280	0.0287	0.0320
Intermediate calculations			
Deg. of freedom	99.000	99.000	99.000
half area of significance	0.025	0.025	0.025
chi-square statistics	77.62	81.54	101.12
Two-Tail Test			
lower critical value	73.361	73.361	73.361
upper critical value	128.422	128.422	128.422
p-value	0.945	0.899	0.422
Results	Do not reject null hypostasis	Do not reject null hypostasis	Do not reject null hypostasis

Table 4.197 *Chi-square variance with the null hypothesis of variance of 0.1% from the baseline of the mean CT measurement with 100 degrees of freedom.*

Chapter 5

CONCLUSION

The use of the dose mass histogram instead of the dose volume histogram is not a new concept. It was first devised in 2005, however, was unable to gain traction[89]. Although based on sound reasoning, technologies like a 4DCT and computing power were too far behind for the idea to be clinically implemented. For example, 4DCT data storage requirements are 10 times that of a regular CT. This combined with the reconstruction of the computer topography, which in 2005 took close to 30-45 minutes per scan would also be increased tenfold. Currently, the reconstruction time for a 4DCT is under 15 minutes and with hardware miniaturization and CT databases like PACS, storage is no longer a hindrance. However, due to this historic lack of availability of resources, the DVH continued and continues to be the evaluation tool for lung radiation. It was well known that the DVH analysis is far from accurate due to the nature of the organ being evaluated and the metrics involved in a dose volume histogram. Clinicians tended to either overcompensate or undercompensate depending on the location and stage of the disease.

Although CT numbers and Hounsfield units were also available in traditional CT scans and could be interpreted for density[22-24], researchers were aware that a single frame CT scan is a snapshot of the lung's and therefore would not be a sensible approach for evaluation of the mass.

With the emergence of fast 4DCTs, this is no longer a restriction; 4DCTs are commonplace procedures in a modern radiation oncology clinic. The use of 4DCT analysis can be used to extract both, the density of lung and volumetric information per phase of the breathing cycle. Using the volume and the density the mass can then be extrapolated for each phase of the breathing cycle. Once the dose is calculated on the entire breathing phase This would be a more representative picture of the radiation actually being delivered to the patient rather than the snapshot dose calculation of the standard CT set.

The other obvious implication is the radiation absorbed dose. All modern radiation treatment planning technology is based on tissue density and its ability to absorb dose along the beam track. Meaning, the denser the tissue is, the more it will absorb the radiation as it penetrates the body and vice versa[26]. Since density is defined as mass per unit volume, the changing density of the lung will also affect the beam track of the incident radiation towards the tumor volume. Those rates of absorption will also affect both the tumor prescribed dose and the toxicity end points. These data will also be gathered and analyzed, by re-computing their delivered plan separately on each phase and then combining them.

What this research effort makes clear is that the use of volumetric metrics in assessing and limiting dose in healthy lung tissue is problematic. It demonstrates that these volumetric dose points change through the patients breathing cycle that continues to change during the course of treatment. This effort also shows a different metric that has the potential to be a more informative to the team providing care to the patient. And finally, it shows that this method is more stable through the patient's breathing cycle than the volume dose point.

The future potentials of this research effort would come to fruition in the form of prospective clinical trials. However, before a prospective clinical trial, a more comprehensive retrospective data set of patient cohorts and follow-ups would be needed. This would require a re-examination on existing patients on other clinical trials for lung cancer therapy to have their four-dimensional CT scans used to extract mass information. This would then be followed by the techniques described in the study to extract dosimetric mass points and then a comprehensive follow-up with the patients to see if a correlation can be found between radiation-induced pneumonitis and the mass of lungs receiving certain doses.

If this correlation is found to be relevant, that a relationship between radiation-induced pneumonitis and the mass of lung irradiated can be proven, then the next step would be to see if the mass of lung irradiated is a better or more stable indicator than the volume of lung irradiated.

Depending on the outcome of this retrospective study, a prospective clinical trial could be set up in which dosimetric constraints in the radiation treatment plans would be governed and limited by the mass of lung irradiated through the course of the patient's treatment. The purpose of this trial would be to determine how much mass of lung can be safely irradiated before the onset of radiation-induced pneumonitis.

BIBLIOGRAPHY

1. Siegel, R.L., K.D. Miller, and A. Jemal, *Cancer Statistics*, 2017. CA Cancer J Clin, 2017. 67(1): p. 7-30.D doi: 10.3322/caac.21387

2. Chapple, A., S. Ziebland, and A. McPherson, Stigma, shame, and blame experienced by patients with lung cancer: qualitative study. *BMJ*, 2004. 328(7454): p. 1470 doi: https://doi.org/10.1136/bmj.38111.639734.7C.

3. Munley, M.T., et al., Multimodality nuclear medicine imaging in three-dimensional radiation treatment planning for lung cancer: challenges and prospects. *Lung Cancer*, 1999. 23(2): p. 105-14. doi: https://doi.org/10.1016/S0169-5002(99)00005-7

4. Kocak, Z., et al., Challenges in defining radiation pneumonitis in patients with lung cancer. Int J Radiat Oncol Biol Phys, 2005. 62(3): p. 635-8. DOI: https://doi.org/10.1016/S0169-5002(99)00005-7 doi: 10.1016/j.ijrobp.2004.12.023

5. Timmerman, R., et al., Excessive toxicity when treating central tumors in a phase II study of stereotactic body radiation therapy for medically inoperable early-stage lung cancer. *J Clin Oncol*, 2006. 24(30): p. 4833-9. doi: 10.1200/JCO.2006.07.5937

6. Hall, E.J. and A.J. Giaccia, Radiobiology for the radiologist. 2019 ISBN-13: 978-1496335418

7. ASTRO, ASTRO – Program Description/Statement of Need. *International Journal of Radiation Oncology Biology Physics*, 2017. Volume 99(Issue 2, Supplement): p. A 8.

8. Hernando, M.L., et al., Radiation-induced pulmonary toxicity: a dose-volume histogram analysis in 201 patients with lung cancer. *Int J Radiat Oncol Biol Phys*, 2001. 51(3): p. 650-9. PMID: 11597805

9. Vagane, R., et al., Radiological and functional assessment of radiation-induced pulmonary damage following breast irradiation. *Acta Oncol*, 2008. 47(2): p. 248-54. doi: 10.1080/02841860701630267

10. Allen, A.M., et al., Fatal pneumonitis associated with intensity-modulated radiation therapy for mesothelioma. *Int J Radiat Oncol Biol Phys*, 2006. 65(3): p. 640-5 doi: 10.1016/j.ijrobp.2006.03.012.

11. Khalil, A.A., et al., New dose constraint reduces radiation-induced fatal pneumonitis in locally advanced non-small cell lung cancer patients treated with intensity-modulated radiotherapy. *Acta Oncol*, 2015. 54(9): p. 1343-9. doi: 10.3109/0284186X.2015.1061216

12. Marks, L.B., et al., Radiation dose-volume effects in the lung. *Int J Radiat Oncol Biol Phys*, 2010. 76(3 Suppl): p. S70-6. DOI: 10.1016/j.ijrobp.2009.06.091

13. Austin-Seymour, M.M., et al., Dose volume histogram analysis of liver radiation tolerance. *Int J Radiat Oncol Biol Phys*, 1986. 12(1): p. 31-5.

14. McNeely, L.K., et al., Dose volume histogram analysis of lung radiation from chest wall treatment: comparison of electron arc and tangential photon beam techniques. *Int J Radiat Oncol Biol Phys*, 1991. 21(2): p. 515-20.

15. Pan, T., et al., 4D-CT imaging of a volume influenced by respiratory motion on multi-slice CT. *Med Phys*, 2004. 31(2): p. 333-40.

16. Ziegenhein, P., et al., Real-time energy/mass transfer mapping for online 4D dose reconstruction. *Sci Rep*, 2018. 8(1): p. 3662.

17. Tyler Watkins, W., et al., Dose to mass for evaluation and optimization of lung cancer radiation therapy. *Radiother Oncol*, 2017. 125(2): p. 344-350.

18. Chen, H., et al., SU-E-T-526: Evaluation of Dose Mapping Errors via Use of a Volume-Based Dose Mapping Method. *Med Phys*, 2012. 39(6Part18): p. 3826-3836.

19. Liu, J., et al., SU-G-BRC-08: Evaluation of Dose Mass Histogram as a More Representative Dose Description Method Than Dose Volume Histogram in Lung Cancer Patients. Vol. 43. 2016. 3628-3628.

20. Nawaz, A.O., et al., SU-E-J-174: Volume Based Analysis of Several Doses Point and Their Relation to Changing Volume in a 4DCT. *Medical Physics*, 2015. 42(6Part10): p. 3305-3305.

21. Petrik, V., et al., Godfrey Hounsfield and the dawn of computed tomography. *Neurosurgery*, 2006. 58(4): p. 780-7; discussion 780-7.

22. Hounsfield, G.N., Computerized transverse axial scanning (tomography): Part I. Description of system. 1973. *Br J Radiol*, 1995. 68(815): p. H166-72.

23. Hounsfield, G.N., Computerized transverse axial scanning (tomography). 1. Description of system. *Br J Radiol*, 1973. 46(552): p. 1016-22.

24. Ambrose, J. and G. Hounsfield, Computerized transverse axial tomography. *Br J Radiol*, 1973. 46(542): p. 148-9.

25. Khan, F.M., Physics of Radiation Therapy. 2012.

26. Khan, F.M. and J.P. Gibbons, Khan's the physics of radiation therapy. 2015.

27. Balter, J.M., et al., Uncertainties in CT-based radiation therapy treatment planning associated with patient breathing. *Int J Radiat Oncol Biol Phys*, 1996. 36(1): p. 167-74.

28. Ekberg, L., L. Wittgren, and O. Holmberg, What margins should be added to the clinical target volume in radiotherapy treatment planning of lung cancer? *Radiotherapy and Oncology*. 37: p. S19.

29. Underberg, R.W., et al., Use of maximum intensity projections (MIP) for target volume generation in 4DCT scans for lung cancer. I*nt J Radiat Oncol Biol Phys, 2005*. 63(1): p. 253-60.

30. Endo, M., et al., Four-dimensional computed tomography (4D CT)--concepts and preliminary development. *Radiat Med*, 2003. 21(1): p. 17-22.

31. Molina, D.K. and V.J. DiMaio, Normal organ weights in men: part II-the brain, lungs, liver, spleen, and kidneys. *Am J Forensic Med Pathol*, 2012. 33(4): p. 368-72.

32. Vedam, S.S., et al., Acquiring a four-dimensional computed tomography dataset using an external respiratory signal. *Phys Med Biol*, 2003. 48(1): p. 45-62.

33. Ford, E.C., et al., Respiration-correlated spiral CT: a method of measuring respiratory-induced anatomic motion for radiation treatment planning. *Med Phys*, 2003. 30(1): p. 88-97.

34. Taguchi, K., Temporal resolution and the evaluation of candidate algorithms for four-dimensional CT. *Med Phys*, 2003. 30(4): p. 640-50.

35. Low, D.A., et al., A method for the reconstruction of four-dimensional synchronized CT scans acquired during free breathing. *Med Phys*, 2003. 30(6): p. 1254-63.

36. Keall, P., 4-dimensional computed tomography imaging and treatment planning. *Semin Radiat Oncol*, 2004. 14(1): p. 81-90.

37. Chen, G.G. and P.B.S. Lai, Apoptosis in carcinogenesis and chemotherapy : apoptosis in cancer. 2009.

38. Melino, G. and D. Vaux, Cell death. 2010, Chichester, UK; Hoboken, NJ: Wiley-Blackwell.

39. McEwen, M., et al., Addendum to the AAPM's TG-51 Protocol for Clinical Reference Dosimetry of High-Energy Photon Beams. Igaku Butsuri, 2017. 37(1): p. 2-24.

40. Kinoshita, N., et al., Comparison of AAPM Addendum to TG-51, IAEA TRS-398, and JSMP 12: Calibration of photon beams in water. *J Appl Clin Med* Phys, 2017. 18(5): p. 271-278.

41. Almond, P.R., et al., AAPM's TG-51 protocol for clinical reference dosimetry of high-energy photon and electron beams. Med Phys, 1999. 26(9): p. 1847-70.

42. Bentel, G.C., Radiation therapy planning. 1996, New York: McGraw-Hill, Health Professions Division.

43. Moorrees, J. and E. Bezak, Four dimensional radiotherapy: a review of current technologies and modalities. *Australas Phys Eng Sci Med*, 2012. 35(4): p. 399-406.

44. Jaffray, D.A., et al., Accurate accumulation of dose for improved understanding of radiation effects in normal tissue. *Int J Radiat Oncol Biol Phys*, 2010. 76(3 Suppl): p. S135-9.

45. Siebers, J.V. and H. Zhong, An energy transfer method for 4D Monte Carlo dose calculation. *Med Phys*, 2008. 35(9): p. 4096-105.

46. Versteijne, E., et al., Considerable interobserver variation in delineation of pancreatic cancer on 3DCT and 4DCT: a multi-institutional study. *Radiat Oncol,* 2017. 12(1): p. 58.

47. Cai, W., et al., 3D delivered dose assessment using a 4DCT-based motion model. *Med Phys,* 2015. 42(6): p. 2897-907.

48. Cole, A.J., et al., Investigating the potential impact of four-dimensional computed tomography (4DCT) on toxicity, outcomes and dose escalation for radical lung cancer radiotherapy. *Clin Oncol (R Coll Radiol)*, 2014. 26(3): p. 142-50.

49. Livingston, G.C., et al., Toxicity and dosimetric analysis of non-small cell lung cancer patients undergoing radiotherapy with 4DCT and image-guided intensity modulated radiotherapy: a regional centre's experience. *J Med Radiat Sci*, 2016. 63(3): p. 170-8.

50. Wilkens, J.J., et al., IMRT treatment planning based on prioritizing prescription goals. *Phys Med Biol*, 2007. 52(6): p. 1675-92.

51. Seco, J., et al., Dosimetric impact of motion in free-breathing and gated lung radiotherapy: a 4D Monte Carlo study of intrafraction and interfraction effects. *Med Phys,* 2008. 35(1): p. 356-66.

52. Bortfeld, T., S.B. Jiang, and E. Rietzel, Effects of motion on the total dose distribution. *Semin Radiat Oncol*, 2004. 14(1): p. 41-51.

53. Piper, J., SU-FF-I-68: Evaluation of An Intensity-Based Free-Form Deformable Registration Algorithm. *Medical Physics*, 2007. 34(6Part3): p. 2353-2354.

54. Rosu, M., et al., Dose reconstruction in deforming lung anatomy: dose grid size effects and clinical implications. *Med Phys*, 2005. 32(8): p. 2487-95.

55. Zhong, H. and J.V. Siebers, Monte Carlo dose mapping on deforming anatomy. *Phys Med Biol*, 2009. 54(19): p. 5815-30.

56. Sohn, M., et al., Model-independent, multimodality deformable image registration by local matching of anatomical features and minimization of elastic energy. *Med Phys*, 2008. 35(3): p. 866-78.

57. Sonke, J.J. and J. Belderbos, Adaptive radiotherapy for lung cancer. *Semin Radiat Oncol*, 2010. 20(2): p. 94-106.

58. Guckenberger, M., et al., Potential of adaptive radiotherapy to escalate the radiation dose in combined radiochemotherapy for locally advanced non-small cell lung cancer. Int J Radiat Oncol Biol Phys, 2011. 79(3): p. 901-8.

59. Drzymala, R.E., et al., Dose-volume histograms. *Int J Radiat Oncol Biol Phys*, 1991. 21(1): p. 71-8.

60. Hasson, B.F., Dose Volume Histogram (DVH), in Encyclopedia of Radiation Oncology, L.W. Brady and T.E. Yaeger, Editors. 2013, Springer Berlin Heidelberg: Berlin, Heidelberg. p. 166-166.

61. Barrett, A., Practical radiotherapy planning. 2009, London: Hodder Arnold.

62. Emami, B., et al., Tolerance of normal tissue to therapeutic irradiation. *Int J Radiat Oncol Biol Phys*, 1991. 21(1): p. 109-22.

63. Miles, E.F., et al., Intensity-modulated radiotherapy for resected mesothelioma: the Duke experience. *Int J Radiat Oncol Biol Phys*, 2008. 71(4): p. 1143-50.

64. Allen Li, X., et al., The use and QA of biologically related models for treatment planning: short report of the TG-166 of the therapy physics committee of the AAPM. Med Phys, 2012. 39(3): p. 1386-409.

65. Bentzen, S.M., et al., Quantitative Analyses of Normal Tissue Effects in the Clinic (QUANTEC): an introduction to the scientific issues. *Int J Radiat Oncol Biol Phys*, 2010. 76(3 Suppl): p. S3-9.

66. Jackson, A., et al., The lessons of QUANTEC: recommendations for reporting and gathering data on dose-volume dependencies of treatment outcome. *Int J Radiat Oncol Biol Phys*, 2010. 76(3 Suppl): p. S155-60.

67. Deasy, J.O., et al., Improving normal tissue complication probability models: the need to adopt a "data-pooling" culture. *Int J Radiat Oncol Biol Phys*, 2010. 76(3 Suppl): p. S151-4.

68. Marks, L.B., et al., Use of normal tissue complication probability models in the clinic. *Int J Radiat Oncol Biol Phys*, 2010. 76(3 Suppl): p. S10-9.

69. Caravatta, L., et al., Inter-observer variability of clinical target volume delineation in radiotherapy treatment of pancreatic cancer: a multi-institutional contouring experience. *Radiation Oncology* (London, England), 2014. 9: p. 198.

70. Carillo, V., et al., Contouring Variability of the Penile Bulb on CT Images: Quantitative Assessment Using a Generalized Concordance Index. *International Journal of Radiation Oncology • Biology • Physics*. 84(3): p. 841-846.

71. Fiorino, C., et al., Intra- and inter-observer variability in contouring prostate and seminal vesicles: implications for conformal treatment planning. *Radiother Oncol*, 1998. 47(3): p. 285-92.

72. Brown, M.S., et al., Method for segmenting chest CT image data using an anatomical model: preliminary results. *IEEE Transactions on Medical Imaging*, 1997. 16(6): p. 828-839.

73. Kadoya, N., et al., Multi-institutional Validation Study of Commercially Available Deformable Image Registration Software for Thoracic Images. Int J *Radiat Oncol Biol Phys*, 2016. 96(2): p. 422-431.

74. Palma, D.A., et al., Predicting radiation pneumonitis after chemoradiation therapy for lung cancer: an international individual patient data meta-analysis. *Int J Radiat Oncol Biol Phys*, 2013. 85(2): p. 444-50.

75. Bradley, J., et al., Toxicity and outcome results of RTOG 9311: A phase I–II dose-escalation study using three-dimensional conformal radiotherapy in patients with inoperable non–small-cell lung carcinoma. *International Journal of Radiation Oncology • Biology • Physics.* 61(2): p. 318-328.

76. Shi, A., et al., Analysis of clinical and dosimetric factors associated with severe acute radiation pneumonitis in patients with locally advanced non-small cell lung cancer treated with concurrent chemotherapy and intensity-modulated radiotherapy. *Radiat Oncol*, 2010. 5: p. 35.

77. Shi, A., et al., Analysis of clinical and dosimetric factors associated with severe acute radiation pneumonitis in patients with locally advanced non-small cell lung cancer treated with concurrent chemotherapy and intensity-

modulated radiotherapy. *Radiation Oncology* (London, England), 2010. 5: p. 35-35.

78. Marks, L.B., et al., Radiation Dose–Volume Effects in the Lung. *International Journal of Radiation Oncology • Biology • Physics*. 76(3): p. S70-S76.

79. Chen, J., et al., Association between absolute volumes of lung spared from low-dose irradiation and radiation-induced lung injury after intensity-modulated radiotherapy in lung cancer: a retrospective analysis. *Journal of Radiation Research*, 2015. 56(6): p. 883-888.

80. Haffty, B.G. and L.D. Wilson, Handbook of radiation oncology : basic principles and clinical protocols. 2009, Sudbury, Mass.: Jones and Bartlett Publishers.

81. Dale, P.J., F.L. Matthews, and R.C. Schroter, Finite element analysis of lung alveolus. *J Biomech*, 1980. 13(10): p. 865-73.

82. Ghista, D.N., A.S. Kobayashi, and N. Davids, Analyses of some biomechanical structures and flows by computer-based finite element method. *Comput Biol Med,* 1975. 5(1-2): p. 119-161.

83. Matthews, F.L. and J.B. West, Finite element displacement analysis of a lung. *J Biomech*, 1972. 5(6): p. 591-600.

84. Pao, Y.C., et al., Finite-element analysis of the strain variations in excised lobe of canine lung. *J Biomech*, 1978. 11(3): p. 91-100.

85. Vawter, D.L., A finite element model for macroscopic deformation of the lung. *J Biomech Eng*, 1980. 102(1): p. 1-7.

86. Tawhai, M.H., et al., CT-based geometry analysis and finite element models of the human and ovine bronchial tree. *J Appl Physiol* (1985), 2004. 97(6): p. 2310-21.

87. Zhang, G., et al., Biomechanical simulation of thorax deformation using finite element approach. *Biomed Eng Online*, 2016. 15: p. 18.

88. Werner, R., et al., Patient-specific finite element modeling of respiratory lung motion using 4D CT image data. *Med Phys*, 2009. 36(5): p. 1500-11.

89. Nioutsikou, E., et al., Reconsidering the definition of a dose-volume histogram. *Phys Med Biol*, 2005. 50(11): p. L17-19.